



저작자표시-비영리-변경금지 2.0 대한민국

이용자는 아래의 조건을 따르는 경우에 한하여 자유롭게

- 이 저작물을 복제, 배포, 전송, 전시, 공연 및 방송할 수 있습니다.

다음과 같은 조건을 따라야 합니다:



저작자표시. 귀하는 원저작자를 표시하여야 합니다.



비영리. 귀하는 이 저작물을 영리 목적으로 이용할 수 없습니다.



변경금지. 귀하는 이 저작물을 개작, 변형 또는 가공할 수 없습니다.

- 귀하는, 이 저작물의 재이용이나 배포의 경우, 이 저작물에 적용된 이용허락조건을 명확하게 나타내어야 합니다.
- 저작권자로부터 별도의 허가를 받으면 이러한 조건들은 적용되지 않습니다.

저작권법에 따른 이용자의 권리는 위의 내용에 의하여 영향을 받지 않습니다.

이것은 [이용허락규약\(Legal Code\)](#)을 이해하기 쉽게 요약한 것입니다.

[Disclaimer](#)

Master's Thesis

Position-sensing by ZCP Filter for
3-Phase Sinusoidal BLDC Motor Controller

Hoichang Jeong

Department of Electrical Engineering

Ulsan National Institute of Science and Technology

2021

Position-sensing by ZCP Filter for 3-Phase Sinusoidal BLDC Motor Controller

Hoichang Jeong

Department of Electrical Engineering

Ulsan National Institute of Science and Technology

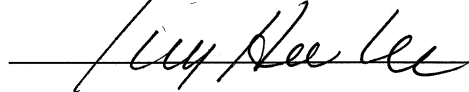
Position-sensing by ZCP Filter for 3-Phase Sinusoidal BLDC Motor Controller

A thesis submitted to
Ulsan National Institute of Science and Technology
in partial fulfillment of the
requirements for the degree of
Master of Science

Hoichang Jeong

12. 15. 2020

Approved by



Advisor

Prof. Myunghee Lee

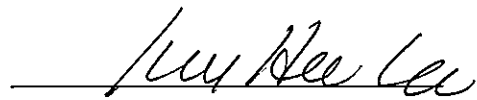
Position-sensing by ZCP Filter for 3-Phase Sinusoidal BLDC Motor Controller

Hoichang Jeong

This certifies that the thesis of Hoichang Jeong is approved.

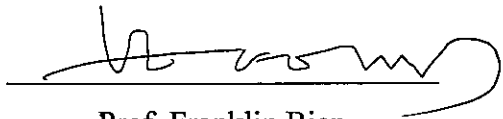
12. 15. 2020

Signature



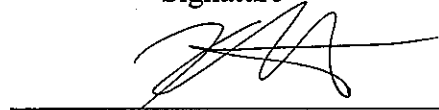
Advisor: Prof. Myunghee Lee

Signature



Prof. Franklin Bien

Signature



Prof. Kyuho Jason Lee

ABSTRACT

In this thesis, studied is a ZCP (Zero Crossing Point) filter scheme along with slow start-up initial driving method for sensor-less 3-phase sinusoidal BLDC (Brush-Less DC Motor) controller. ZCP filter is a key IP block to detect the rotor position of the BLDC motor and control the driving transistors of an inverter.

A traditional 3-phase sinusoidal BLDC motor uses 3 hall sensors to detect the rotor position to control the motor speed. In this case, hall sensors are installed inside a BLDC motor. But it often causes reliability problem in automotive applications due to malfunction of the sensor. Therefore, sensor-less BLDC motor becomes more desirable and the position detection scheme replacing the hall sensor is key area of research.

The proposed digital ZCP filter for the rotor position detection alone with a slow start-up initial driving is implemented by digital logic designed by using Verilog HDL. Also, SPWM (Sinusoidal Pulse Width Modulation) sensor-less BLDC motor controller is designed by Verilog HDL. All function is implemented and verified by using a FPGA.

KEYWORD: Automotive IC, BLDC Motor, SPWM Sensor-less, Position-sensing Digital ZCP Filter, Slow Start-up Initial Driver

CONTENTS

1. Introduction.....	1
1.1 Basic Operation of Sinusoidal PWM BLDC Motor Controller	1
1.2 Design of SPWM BLDC Motor Controller.....	3
1.2.1 Bipolar SPWM Control Condition.....	3
1.2.2 Bipolar SPWM Control with Digital Logic	8
1.3 The Problem of SPWM Sensor-less Control of BLDC Motor	12
2. Proposed Design of Position-sensing ZCP Filter.....	14
2.1 Design of Position-sensing Digital ZCP Filter for Modulation	14
2.2 Design of Position-sensing Digital ZCP Filter for Overmodulation and Six-step.....	19
2.3 Schematic of Position-sensing Digital ZCP Filter	21
2.4 Design of Slow Start-up Initial Driving	22
2.4.1 Initial Driving 1 st Stage: Alignment Stage	23
2.4.2 Initial Driving 2 nd Stage: Acceleration Stage.....	29
2.4.3 Initial Driving TOP Block Diagram.....	30
2.5 TOP Block Diagram of SPWM Sensor-less BLDC Controller	31
3. Simulation and Experiment Results.....	32
3.1 Simulation Results	32
3.2 Experiment Setup.....	34
3.3 Experiment Results	36
4. Conclusion	40
5. Future Works	41

LIST OF FIGURES

Fig. 1.1 Structure and equivalent circuit of BLDC motor.....	2
Fig. 1.2 Equivalent circuit of 3-phase-inverter and BLDC motor	2
Fig. 1.3 Description of bipolar SPWM control.....	3
Fig. 1.4 Description of amplitude and frequency of fundamental wave and carrier wave	4
Fig. 1.5 The relationship between the fundamental and its harmonics	6
Fig. 1.6 Fundamental component of phase voltage of 3-phase-inverter	6
Fig. 1.7 Description of bipolar SPWM control in overmodulation.....	7
Fig. 1.8 Block diagram of period detector	8
Fig. 1.9 Bipolar SPWM control implemented with digital logic	9
Fig. 1.10 Block diagram of sinewave generator and triangular wave generator.....	9
Fig. 1.11 Generating SPWM pulse and high-side and low-side signals	10
Fig. 1.12 Dead-time control finite state machine and state diagram.....	10
Fig. 1.13 Top block diagram of bipolar SPWM BLDC motor controller	11
Fig. 1.14 Circuit and signal of back-EMF difference method	13
Fig. 1.15 Circuit block diagram and signal of zero-sequence voltage method	13
Fig. 2.1 ON pulse of phase voltage in natural sampling method	16
Fig. 2.2 ON pulse of phase voltage in symmetric regular sampling method	16
Fig. 2.3 Algorithm flowchart of position-sensing digital ZCP filter for bipolar SPWM control in modulation	18
Fig. 2.4 Working of position-sensing digital ZCP filter for bipolar SPWM control in modulation....	18
Fig. 2.5 Algorithm flowchart of position-sensing digital ZCP filter for bipolar SPWM control in overmodulation	20
Fig. 2.6 Working of position-sensing digital ZCP filter for bipolar SPWM control in overmodulation	20
Fig. 2.7 Schematic of position-sensing digital ZCP filter.....	21
Fig. 2.8 Overall operation and speed curve of proposed initial driving.....	22
Fig. 2.9 Switching operation of the 3-phase-inverter in alignment stage. (a) is previous alignment stage operation and (b) is proposed alignment stage operation.....	24
Fig. 2.10 PWM signal generating operation used in alignment stage.....	25
Fig. 2.11 Graph of torque and angular speed of the BLDC motor.....	26
Fig. 2.12 Switching step of alignment stage	27
Fig. 2.13 Increase of speed and duty in the alignment stage.....	28

Fig. 2.14 Speed graph and step sequence in acceleration stage	29
Fig. 2.15 Initial driving TOP block diagram	30
Fig. 2.16 SPWM sensor-less BLDC motor controller TOP block diagram	31
Fig. 3.1 Simulation of position sensing digital ZCP filter for modulation.....	32
Fig. 3.2 Simulation of position sensing digital ZCP filter for overmodulation.....	33
Fig. 3.3 Simulation of slow start-up alignment stage & acceleration stage	33
Fig. 3.4 Test board of the experiment	35
Fig. 3.5 Block diagram of experiment setup.....	35
Fig. 3.6 Getting virtual hall sensor signal by position-sensing digital ZCP filter for modulation. (a) is modulation control and (b) is enlarged figure of (a).....	36
Fig. 3.7 Getting virtual hall sensor signal by position-sensing digital ZCP filter for overmodulation and six-step. (a) is six-step control and (b) is filtering interval	37
Fig. 3.8 Getting virtual hall sensor signal by position-sensing digital ZCP filter for six-step and overmodulation. (a) is overmodulation control and (b) is filtering interval.....	38
Fig. 3.7 High-side gate control signals in slow start-up initial driving. (a) is high-side gate control signals and (b) is enlarged GATE_UH signal in (a).....	39
Fig. 5.1 Proposed SPWM sensor-less BLDC controller applying with PID controller	41

LIST OF TABLES

Table 1.1 Pros and cons of six-step control and PWM control.....	2
Table 3.1 Specification of BLDC motor (BD42) used in the experiment.....	34
Table 3.2 Specification of 3-phase-inverter (HIP2103-4DEMO2Z) used in the experiment.....	34

GLOSSARY

DC	Direct Current
AC	Alternating Current
BLDC	Brush-less Direct Current
PWM	Pulse Width Modulation
SPWM	Sinusoidal Pulse Width Modulation
ZCP	Zero Crossing Point
EMF	Electromotive Force
THD	Total Harmonic Distortion
FPGA	Field Programmable Gate Array
RPM	Revolution Per Minute

1. Introduction

The BLDC (Brush-less DC) motor, used in many industrial applications, is a motor that improves the lifespan and performance of a DC motor [1]. Conventional DC motors have a brush that supplies current to a commutator, which is in contact with commutator and worn away by friction every time it rotates. This brush is related to the lifespan of the DC motor, and BLDC motor was proposed to solve this problem. The BLDC motor has high efficiency, reliability, less noise, and high torque than the brushed DC motor [2]. In order to operate the BLDC motor, the position of the rotor must be detected using hall sensors and the switching time shall be determined from there [3]. However, it may be necessary to lower the price of the BLDC motor by reducing the installation cost of the hall sensor inside the motor [4]. Also, the distance between the inverter circuit and the BLDC motor is too distant to use the hall sensor signals. Moreover, in sensor-based control, the BLDC motor cannot be operated if the hall sensor has trouble. To solve this problem requires sensor-less driving to drive BLDC motor without hall sensors, and many methods for this have been proposed [5]-[10].

1.1 Basic Operation of Sinusoidal PWM BLDC Motor Controller

The BLDC motor is controlled by 3-phase-inverter which converts DC to AC as shown in Fig 1.2 and Fig 1.3. The basic driving principle of the BLDC motor is to change the phase windings, which should be excited according to the position of the rotor for producing continuous torque [11]. To implement this function, information about the rotor position is indispensable [11]. The position can be achieved from the hall sensors. Three output signals of hall sensors enable BLDC motor controller to recognize the rotor position divided into six different sections [11]. The principle of the BLDC motor control is to turn the switches of the 3-phase-inverter on and off according to the six sections and to control the electromagnetic force of the stator to rotate the rotor.

There are two methods of control: six-step control and PWM control. The six-step control has the advantage of being simple [12]. However, the six-step control has ripple in the torque and current. It also has a little noise in operation [12]. In other words, the PWM control is more complex control method than the six-step control. Nevertheless, the PWM control has less ripple in torque and current than six-step control [12]. Moreover, it has less noise compared to the six-step control [12]. Specific advantages and disadvantages of six-step and PWM control are organized in Table 1.2. In this design, SPWM (Sinusoidal PWM) control method is used for lower torque ripple and current ripple.

Table. 1.1 Pros and cons of six-step control and PWM control

	Six-step control	PWM control
Using coil	Only 2 coils used	All 3 coils used
Torque ripple	Worse	Better
Noise	Worse	Better
Dead-time control	Not required	Required
Circuit implementation complexity	Simple	Complex

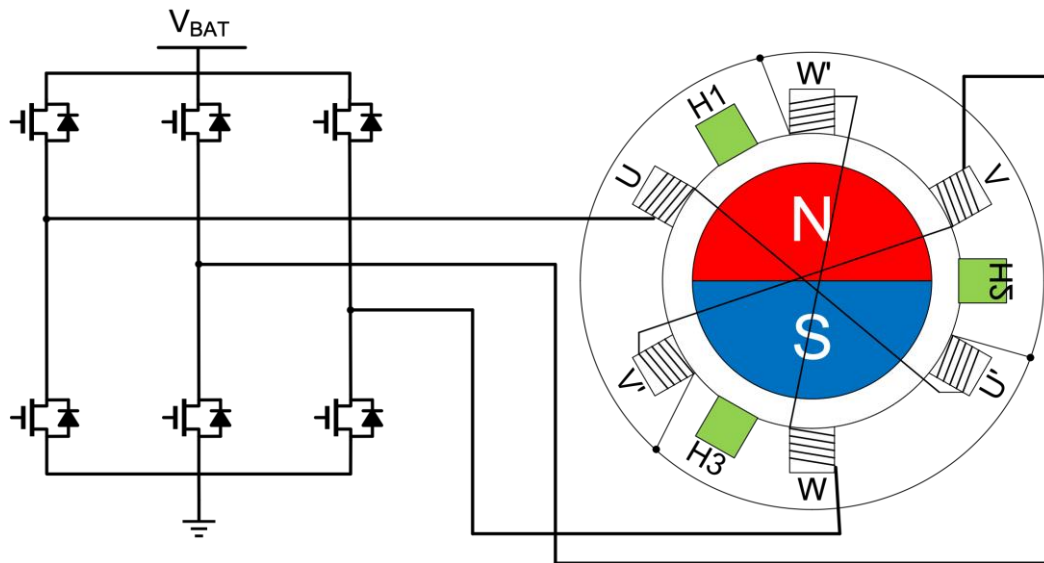


Fig. 1.1 3-phase-inverter and BLDC motor

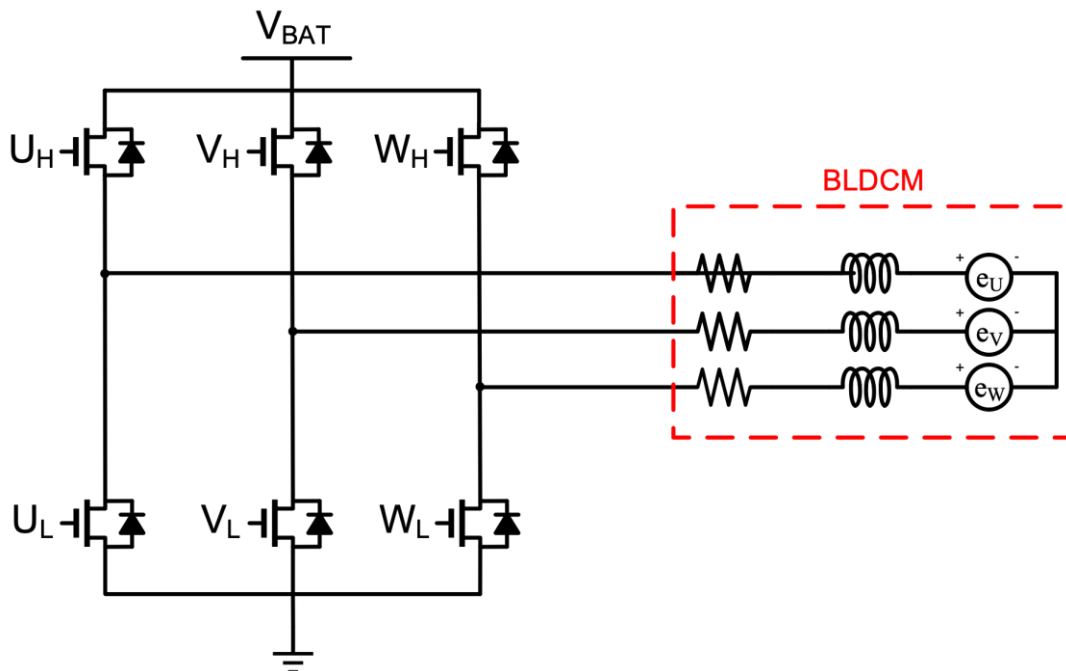


Fig. 1.2 Equivalent circuit of 3-phase-inverter and BLDC motor

1.2 Design of SPWM BLDC Motor Controller

1.2.1 Bipolar SPWM Control Condition

The switching signal is made in the bipolar SPWM method by comparing fundamental waves and carrier waves [13]. As shown in Fig. 1.3, the bipolar SPWM method uses sinewave as the fundamental wave and the triangular wave as the carrier wave. In bipolar SPWM, if the fundamental wave is greater than the carrier wave, the switching signal becomes high-level. Otherwise, it becomes low-level. The created switching signal turns on and off the high-side and low-side switches of the half-bridge and corresponds to the half-bridge terminal voltage (phase voltage) [13]. This terminal voltage is used as input of the BLDC motor.

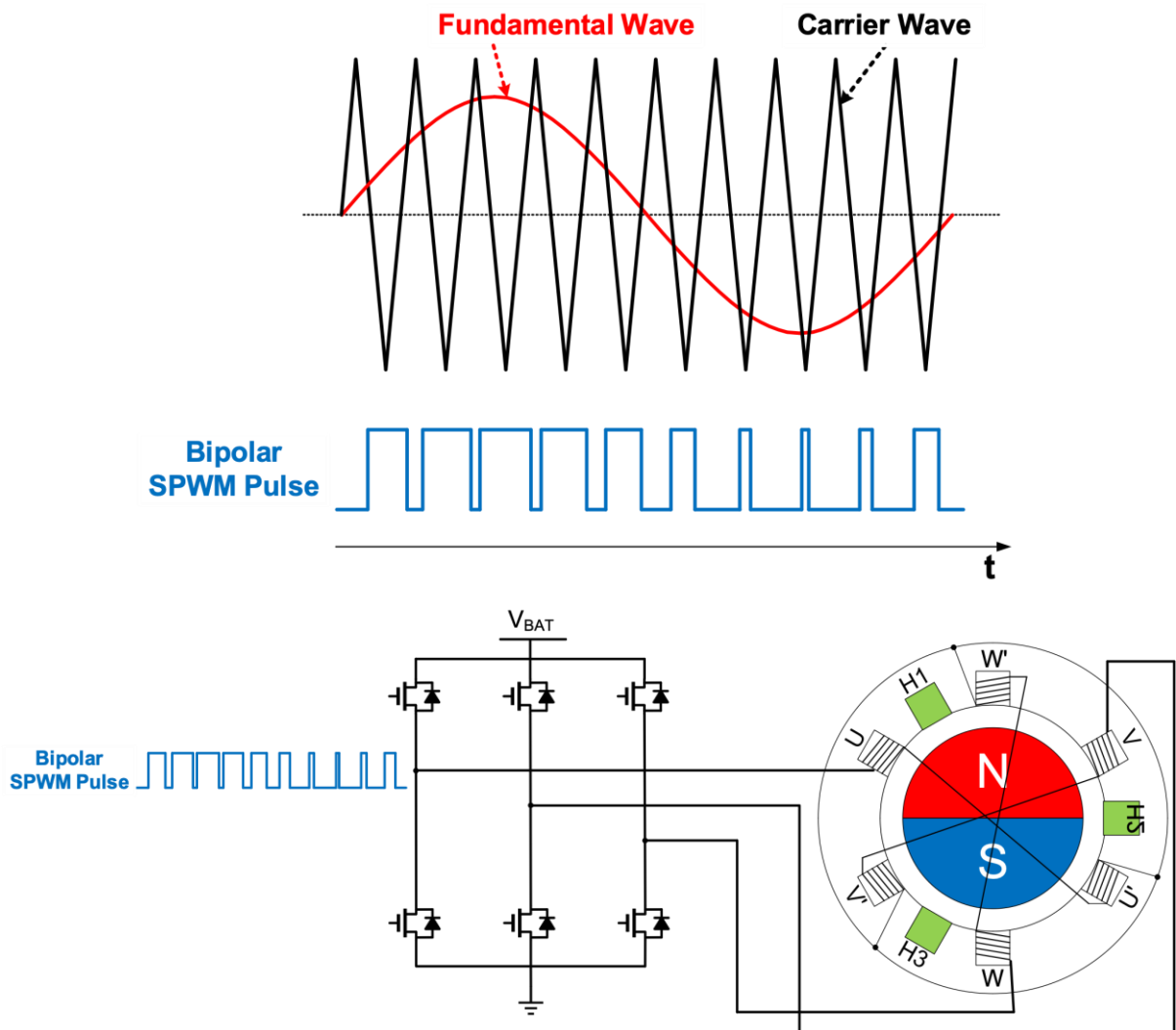


Fig. 1.3 Description of bipolar SPWM control.

Two factors should be considered for driving the BLDC motor in the bipolar SPWM control. The first is the modulation index, MI, which indicates the voltage utilization level, also known as the amplitude modulation ratio. It is defined as in (1) [14].

$$MI = m_a = \frac{V_{PP,F}}{V_{PP,C}} \quad (1)$$

The second is the frequency modulation ratio, m_f , which describes the quality of the current waveform [11]. It is defined as in (2) [16].

$$m_f = \frac{f_C}{f_F} \quad (2)$$

The modulation index is determined by the relationship of amplitude between the fundamental wave and the carrier wave. The bipolar SPWM method uses the triangle wave as the carrier wave and sine wave as the fundamental wave. The closer the amplitude of the triangle wave and the amplitude of the sine wave, the closer the MI approaches 1.

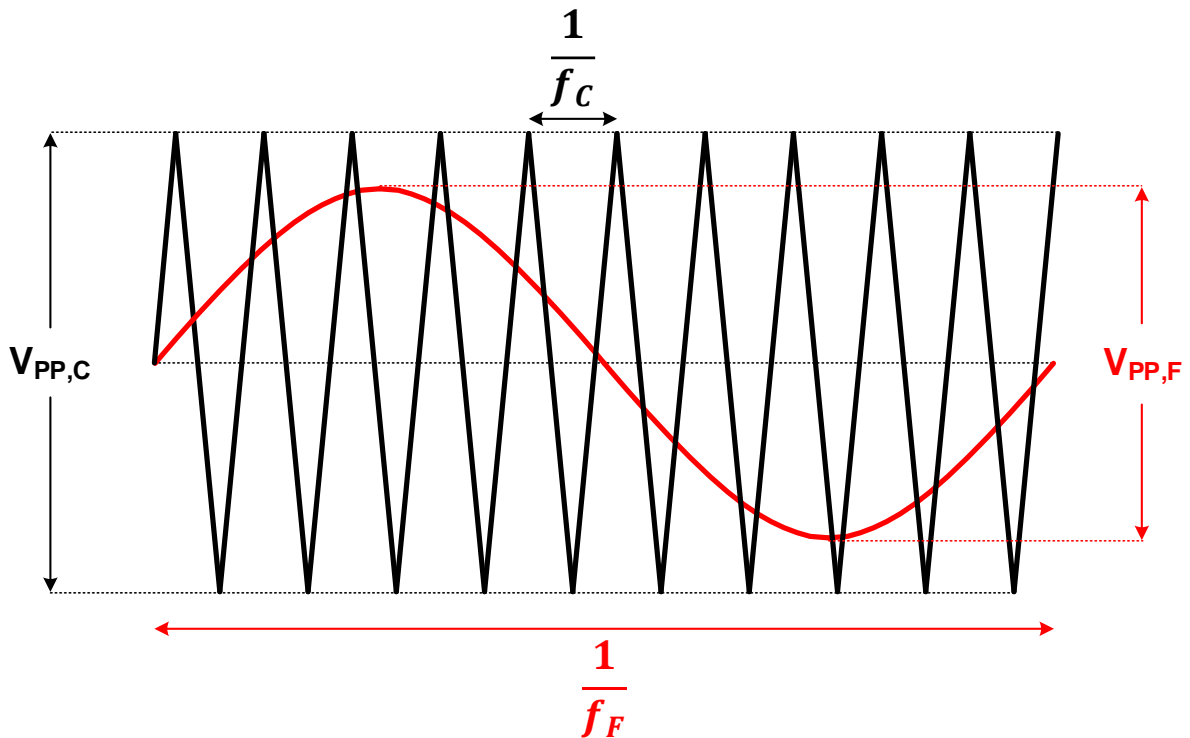


Fig. 1.4 Description of amplitude and frequency of fundamental wave and carrier wave.

As the modulation index nears 1, total harmonic distribution (THD) of the BLDC motor can be reduced, which is related to peak currents and core loss in motors. THD can be expressed as in (3).

$$THD = \frac{\sqrt{V_2^2 + V_3^2 + V_4^2 + \dots + V_N^2}}{V_1} \quad (3)$$

Where V_N is the RMS voltage of Nth harmonic and $N = 1$ is the fundamental harmonic.

From the equation (3), THD can be modified as equation (4).

$$THD = \frac{\sqrt{\Sigma V_{total}^2 - V_1^2}}{\sqrt{V_1^2}} \quad (4)$$

As V_1 is the term of the fundamental frequency, therefore, V_1 can be described as (5).

$$V_1 = \frac{MI}{\sqrt{2}} \cdot V_{BAT} \quad (5)$$

Where V_{BAT} is power voltage of 3-phase-inverter. As a result, we get the below equation about THD as (6).

$$THD = \frac{\sqrt{\Sigma V_{total}^2 - V_1^2}}{\sqrt{V_1^2}} = \sqrt{\frac{\Sigma V_{total}^2}{\left(\frac{MI}{\sqrt{2}} \cdot V_{BAT}\right)^2} - 1} \quad (6)$$

Therefore, if V_{BAT} is assumed to remain unchanged, then, the greater the MI, the lower the THD, the inverse relationship between MI and THD. Lower THD implies lower peak current, less heating, and less core loss in motor [17]. However, if $V_{pp,F}$ is greater than $V_{pp,C}$ then the MI is greater than 1; and if the MI is greater than 1, overmodulation occurs. At this time, the switching signal will contain more harmonic component. As a result, the THD grows again and increases the peak current, heating, and core loss [17].

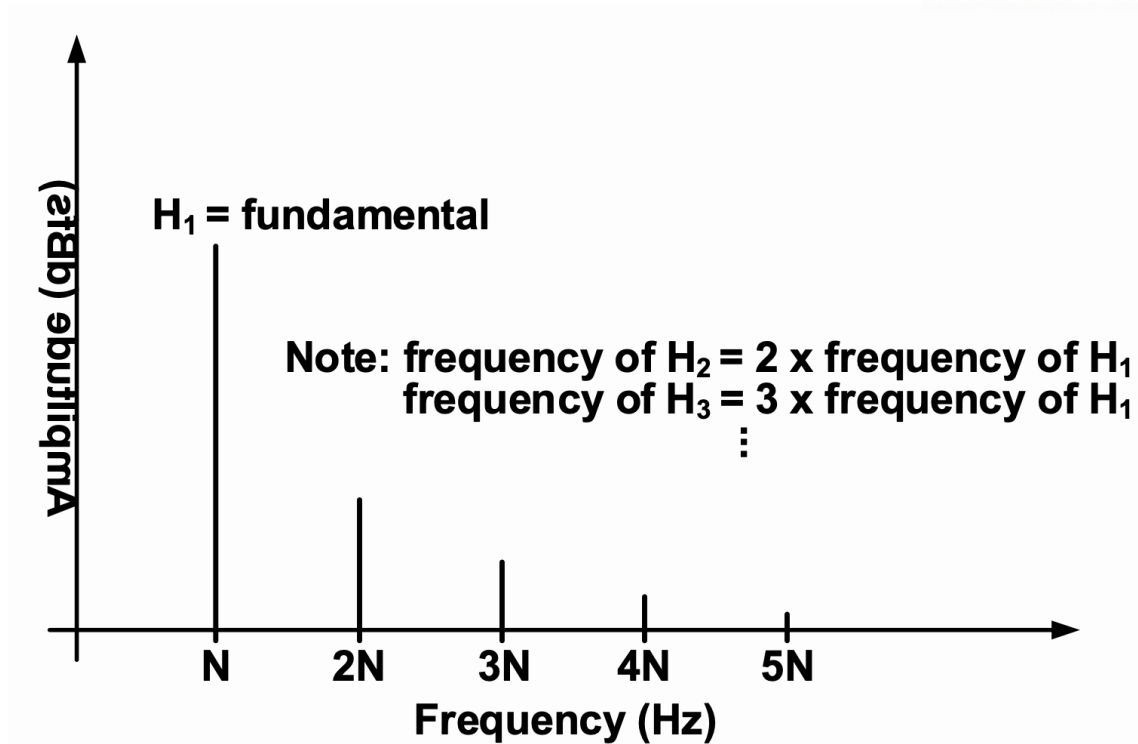


Fig. 1.5 The relationship between the fundamental and its harmonics.

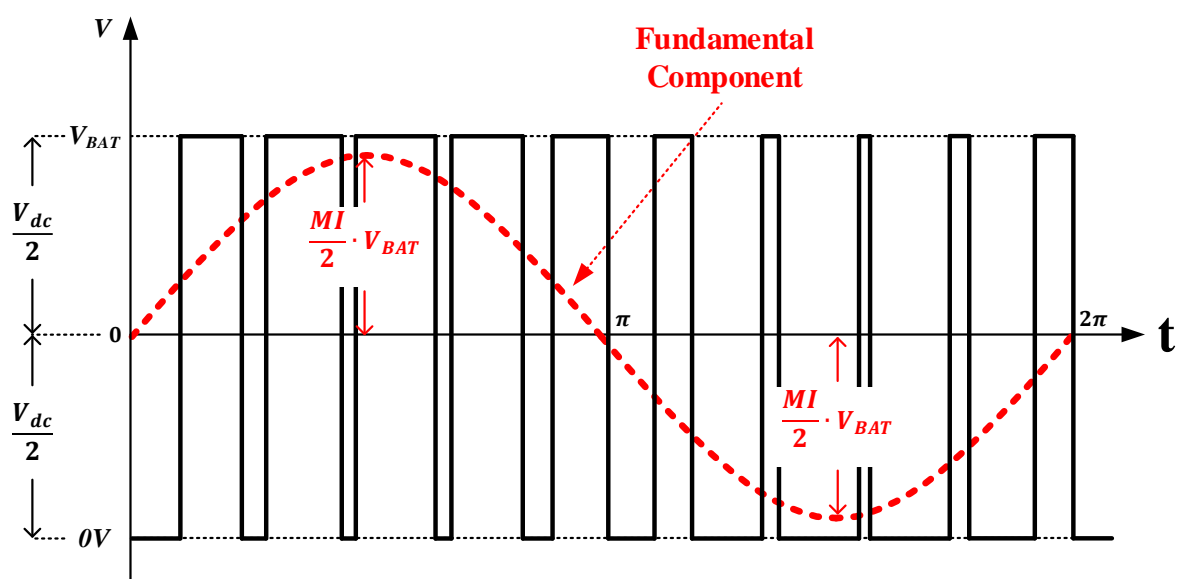


Fig. 1.6 Fundamental component of phase voltage of 3-phase inverter.

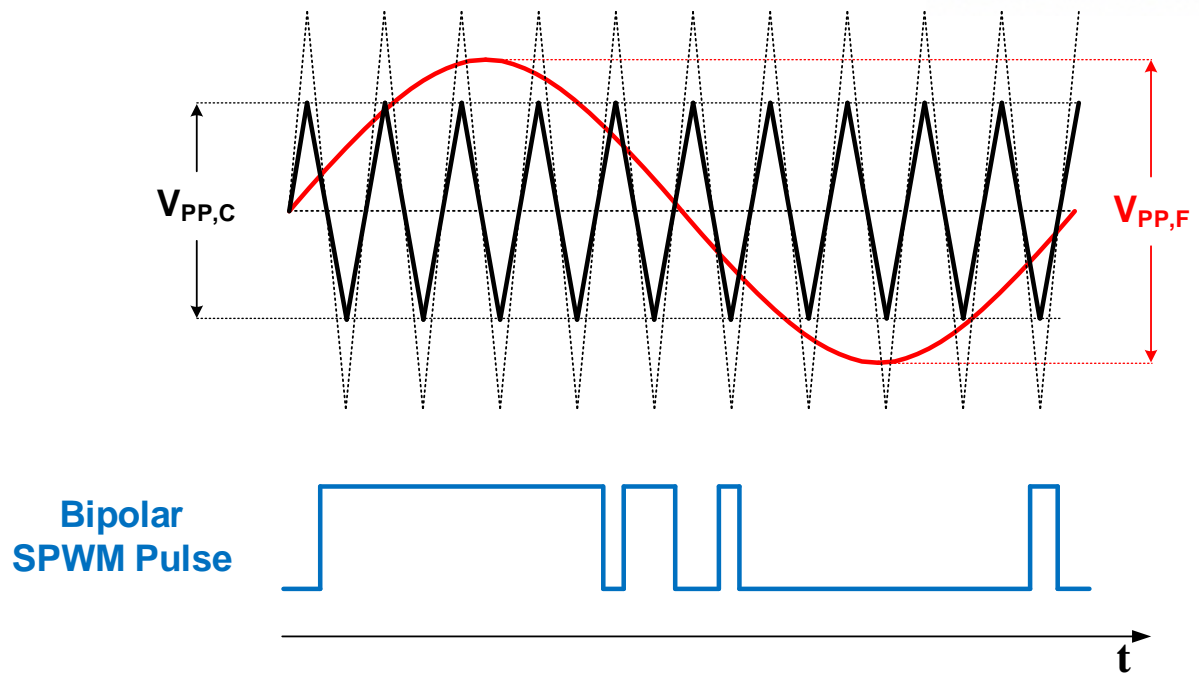


Fig. 1.7 Description of bipolar SPWM control in overmodulation.

The frequency modulation ratio is determined by the frequency relationship between the fundamental wave and the carrier wave. If the frequency of the fundamental wave is higher than that of the carrier wave, the quality of the voltage waveform can be improved [11]. Also, f_c shall be three times of the f_f . This is because the line-to-line voltage of the 3-phase-inverter is the difference between the two terminal voltages, and if m_f is three times the number then there is no phase difference in the harmonics of the terminal voltage. Therefore, if m_f is triple the amount, the THD will decrease with the removal of the harmonics of line-to-line voltage [11]. SPWM control, which includes these amplitude and frequency conditions, reduces the THD of the BLDC motor, thereby reducing the torque ripple of the motor to increase performance.

1.2.2 Bipolar SPWM Control with Digital Logic

Bipolar SPWM control is implemented as digital logic using Verilog HDL language. The SPWM control block consists of several digital sub-blocks. First, a period detector calculates the time required for the BLDC motor to turn around once. Second, there is a sinewave generator that makes address according to the position and RPM of the motor and sinewave that will be used as a fundamental wave based on this address. Third, there is a triangular wave generator that makes triangular wave to be used as carrier wave. Fourth, a bipolar SPWM pulse generator makes a SPWM pulse by comparing the fundamental wave and the carrier wave. Finally, the dead-time controller makes 3-phase-inverter gate input signals through dead-time control. These five blocks will come together to make a bipolar SPWM driver, and each will explain its function for the block.

A period detector is a block that reads the speed of the rotor from hall sensor signals. In the existing BLDC motor, there are three hall sensors inside that read the S pole of the rotor at intervals of 120° each. The hall sensor produces a signal with a value of 1 (High) facing the S pole and 0 (Low) facing the N pole. The three hall sensors produce constant signals and a constant step called 6-step according to the rotation direction of the rotor. The period detector receives the hall sensor signals as input. It has a constant $360^\circ \cdot (\frac{2}{N})$ cycle, where N is the number of rotor poles. In other words, the hall sensor signal cycle can be expressed in terms of time, and the time taken for the rotor to turn around can be obtained. The period detector uses the counter to indicate the frequency of the hall sensor signal in relation to time. To achieve more accurate speed, the average of the periods obtained from the three hall sensors was calculated to derive the period of the one cycle of rotor. Afterwards, the period detector sends the obtained period value of cycle and period set that indicates the change of the step of hall sensor signals to the sinewave generator.

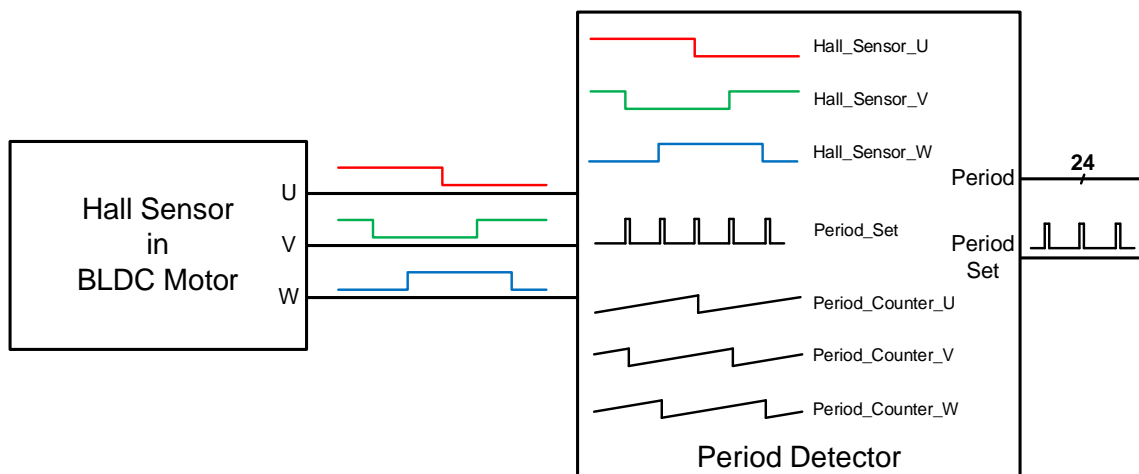


Fig. 1.8 Block diagram of period detector.

The sine wave generator, which creates the sine wave according to the position and period of cycle of the rotor, is divided into two blocks. The first is the "Address Generator" block. This block produces a 10-bit address depending on the RPM and the location of the rotor. Within the block, the position of the rotor can only be expressed at 60° intervals according to the hall sensors, so the address is determined at every sixth step. The address divided by six has a difference of 170 bits, which is 1024 bits divided by six. Afterwards, increase the address during the interval time of period/6 between steps. The created address is used to create the quarter sine wave. The second is the "Quarter Sine wave Generator" block. This block uses the built-in look-up table to create a sine wave from 0 to $\frac{\pi}{2}$, depending on the generated address generated. Amplitude of sine wave consists of 10-bit. The third is the "Full Sine wave Generator" block. The block makes full sine wave using the previously made quarter sine wave. The 10-bit sine wave made in this way will be used as the fundamental wave of bipolar SPWM control.

The triangular wave generator produces a triangular wave using clocks and amplitude trimming that enter the input. The input block affects the frequency of the triangular wave, and amplitude trimming affects amplitude. Also, in this digital logic, the amplitude of the fundamental wave is fixed, so the MI can be modulated by adjusting the amplitude of the triangular wave.

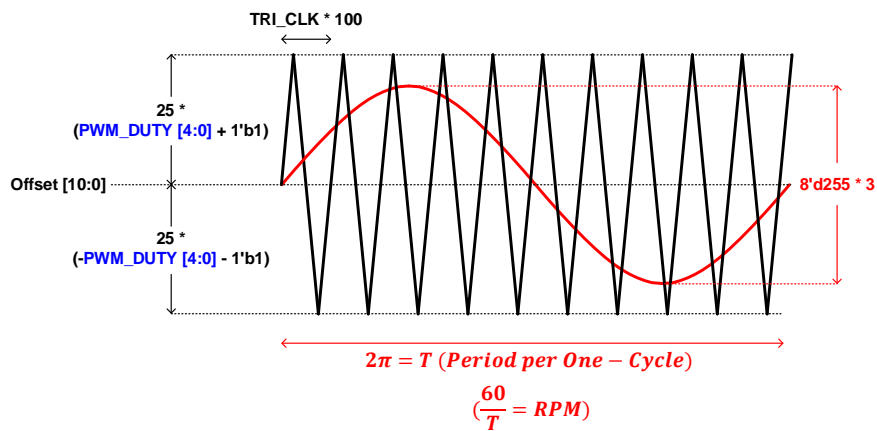


Fig. 1.9 Bipolar SPWM control implemented with digital logic.

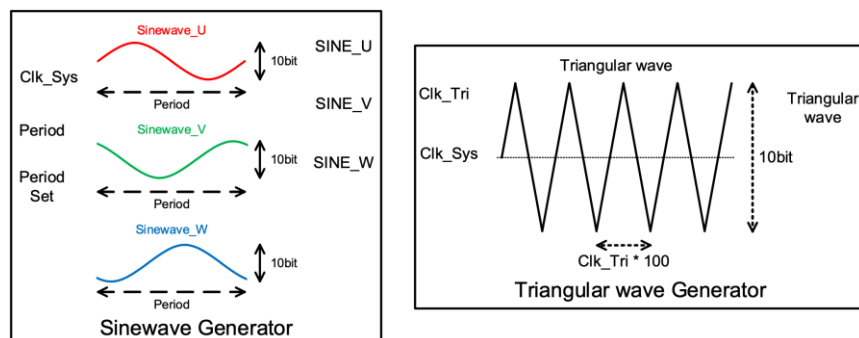


Fig. 1.10 Block diagram of sinewave generator and triangular wave generator.

The bipolar SPWM pulse generator compares the fundamental wave made in the sinewave generator with the carrier wave made in the triangular wave generator to produce the SPWM pulse. If the fundamental wave is greater than the carrier wave, the SPWM pulse has a high level (V_{BAT}). Otherwise, the SPWM pulse has a low level (GND). The generated SPWM pulse is used as a signal of the high-side switch, and the pulse that turns it vertically is used as a signal of the low-side switch. At this time, dead-time control is essential to prevent shoot-through current that occurs when the high-side switch and the low-side switch are simultaneously turned on in one half-bridge circuit. In dead-time controller, the interval between the high-side switch and the low-side switch is adjusted according to the trimming value, and the adjusted high-side signal and low-side signal are sent to their respective switches.

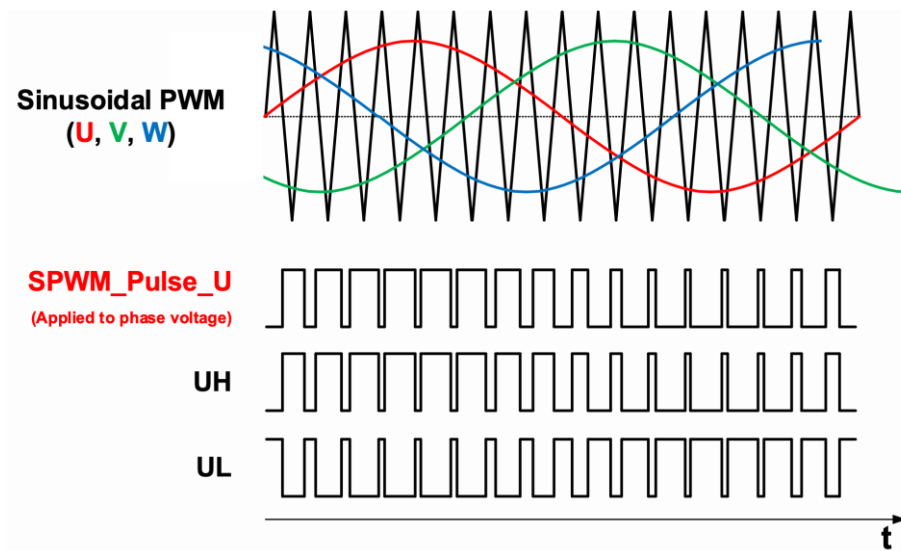


Fig. 1.11 Generating SPWM pulse and high-side and low-side signals.

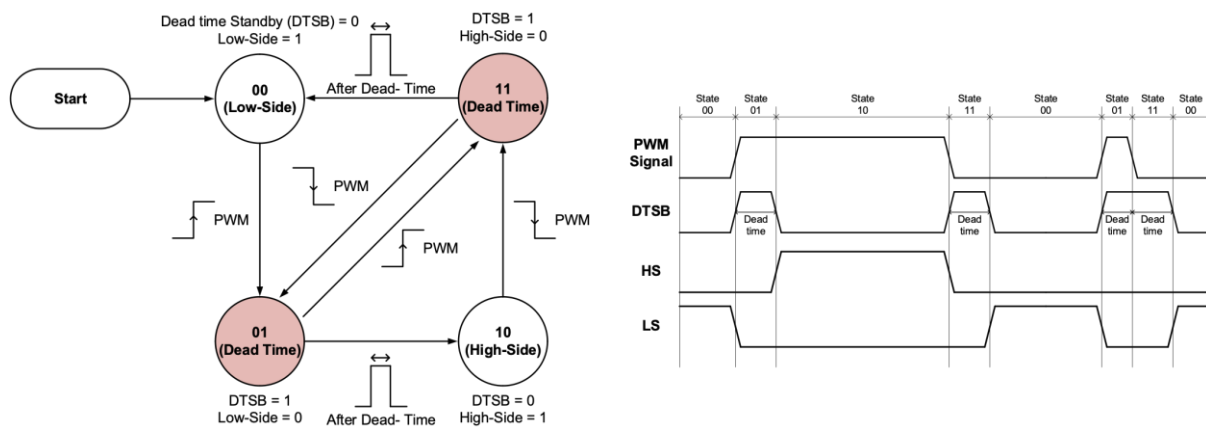


Fig. 1.12 Dead-time control finite state machine and state diagram.

Fig. 1.13 represents the top block diagram of bipolar SPWM BLDC motor controller. The overall operation of the bipolar SPWM BLDC motor controller is as follows. After the location of the rotor is derived from hall sensor signals built into the BLDC motor, determine the rotation cycle of the BLDC motor. From hall sensor signals and rotation cycle, the controller create sinewave to be used as fundamental wave and triangular wave to be used as carrier wave. And, compare the two waves to make an SPWM pulse. The SPWM pulse is created as a gate control signal of a 3-phase-inverter through dead-time control. However, bipolar SPWM control is possible only when there are hall sensor signals used as rotor position information from the hall sensor of the BLDC motor. At the sensor-less BLDC motor, position information of the rotor should be obtained without the hall sensor. In this design, virtual hall sensor signals that indicate the position of the rotor are generated from the phase voltages. The proposed position-sensing digital ZCP filter to be described can obtain virtual hall sensor signals from using phase voltages. Moreover, initial driving system for starting up sensor-less control is necessary. In this design, we designed not only a position-sensing digital ZCP filter but also a slow start-up initial driving block for sensor-less control.

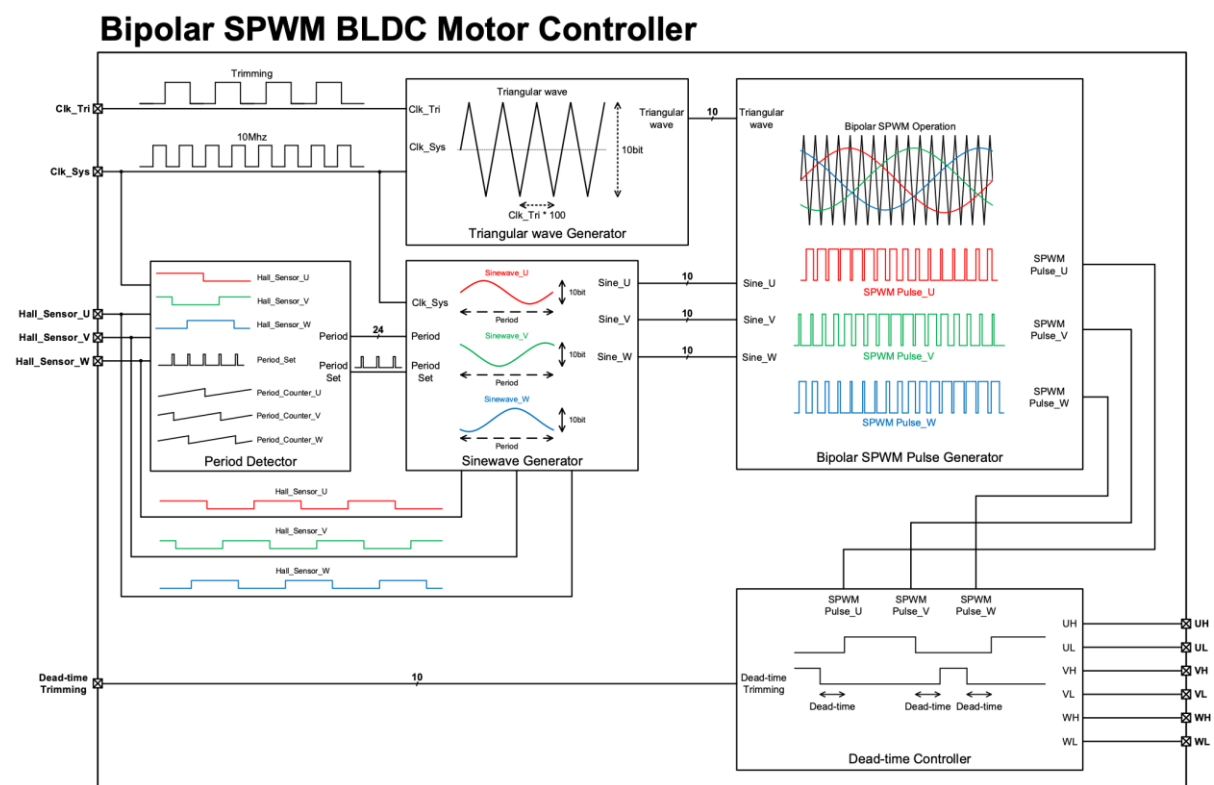


Fig. 1.13 Top block diagram of bipolar SPWM BLDC motor controller.

1.3 The Problem of SPWM Sensor-less Control of BLDC Motor

There are several position-sensing techniques in the sensor-less control technique for determining the position of the rotor without using hall sensors in the BLDC motor [5]-[10]. Various position-sensing techniques include a method of detecting and using the back-EMF of the armature winding, a method of detecting and using the third harmonic of the back-EMF, and a method of detecting and using the current flowing through the freewheeling diode of the phase not operated by the inverter. Among them, most position-sensing techniques use the method of determining the location of the rotor by reading back-EMF. Among them, the back-EMF difference method [18] indirectly obtains the back-EMF by subtracting the phase voltages of different phases from U, V, and W to obtain the back-EMF in the phase voltage. Another, the zero-sequence voltage method [19], detects back-EMF by adding the phase voltages of U, V, and W of different phases to detect the back-EMF inside the phase voltage. Afterwards, noise generated in the commutation section is removed and used as a virtual hall sensor signal. In the case of the back-EMF difference method and the zero-sequence voltage method, since both methods require the calculation of the phase voltage, an op-amp is essential. If any of the op-amps malfunction, the position-sensing circuit cannot perform addition and subtraction operations properly. Moreover, both methods can obtain the back-EMF that occurs in the case of six-step, but it is very difficult to obtain it in the case of SPWM.

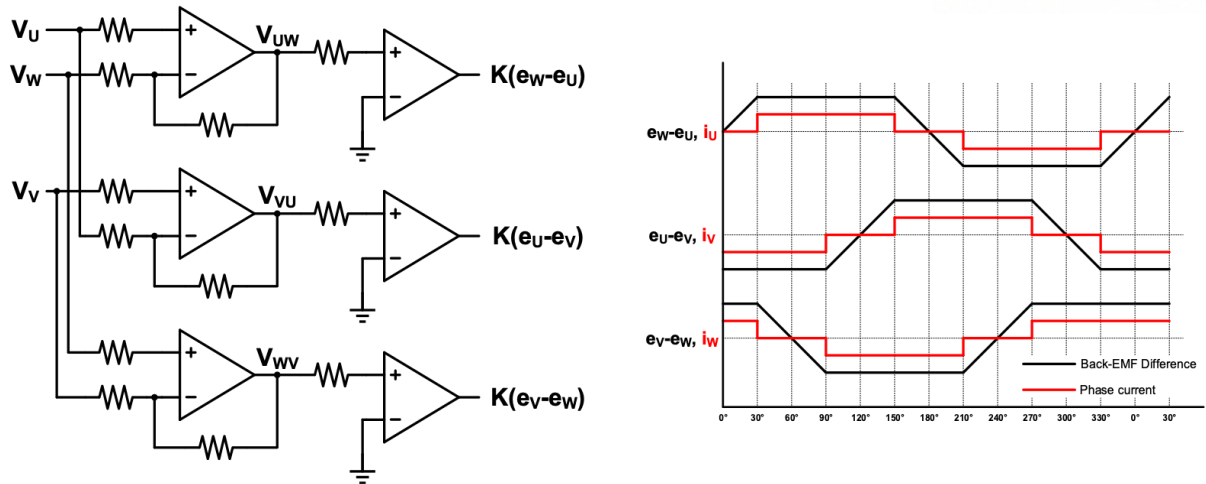


Fig. 1.14 Circuit and signal of back-EMF difference method.

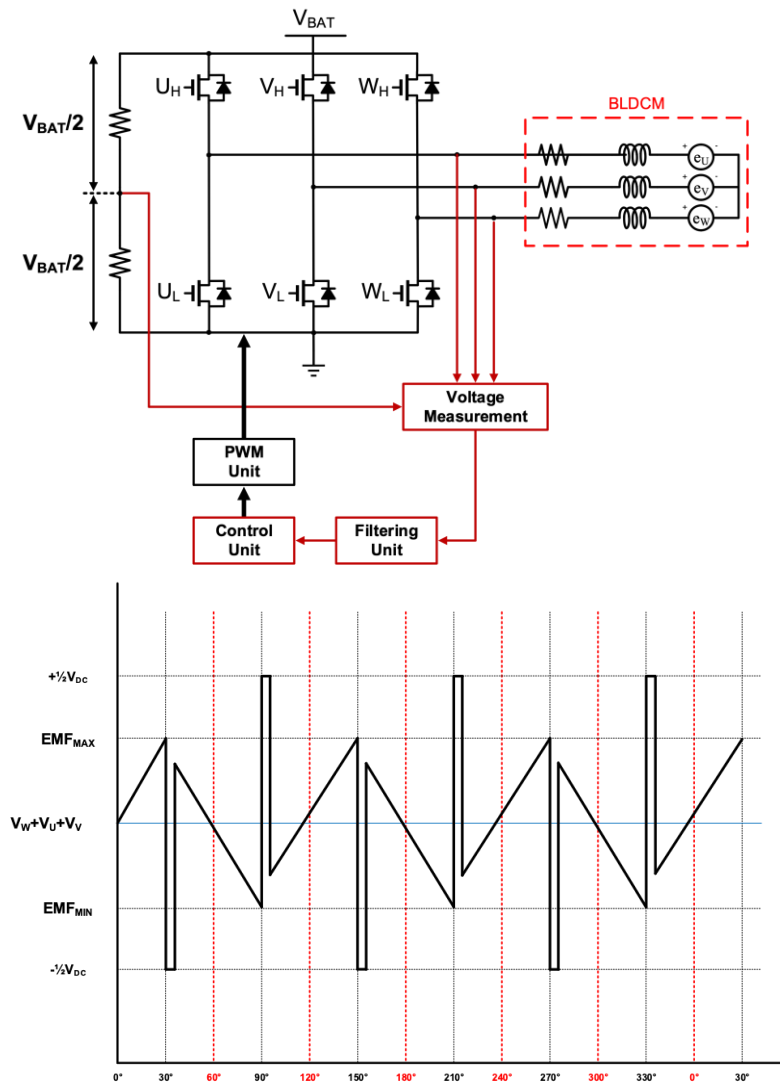


Fig. 1.15 Circuit block diagram and signal of zero-sequence voltage method.

2. Proposed Design of Position-sensing ZCP Filter

For SPWM sensor-less control, the proposed position-sensing digital ZCP filter uses the characteristic that sensor-less control can be applied only when the BLDC motor rotates at a certain speed or more (approximately 1000 to 2000 rpm). The position-sensing digital ZCP filter creates virtual hall sensor signals that inform the position of the rotor using phase voltages. For SPWM sensor-less control and six-step sensor-less control, position-sensing digital ZCP filter is made up of two cores. The first core operates in SPWM modulation, and the second core operates in SPWM overmodulation and six-step.

2.1 Design of Position-sensing Digital ZCP Filter for Modulation

In order to obtain a virtual hall sensor signal using the terminal voltage of 3 phase inverter, the terminal voltage must be expressed as an equation. The expression of terminal voltage can be obtained through the native sampling method. Assuming that T_C is the period of triangular carrier waveform, there are two intersections in one carrier period T_C , t_1 and t_2 . The “ON” duration of each SPWM pulse t_{on1} , t_{on2} are then determined as follows [16]:

$$t_{on1} = \frac{T_C}{4} (1 + m_a \cdot \sin(\omega t_1)) \quad (7)$$

$$t_{on2} = \frac{T_C}{4} (1 + m_a \cdot \sin(\omega t_2)) \quad (8)$$

Where $\omega = \frac{2\pi}{T}$ and T is the period per cycle. The pulse width of the generated SPWM wave in one period is then derived as follows:

$$t_{on} = t_{on1} + t_{on2} = \frac{T_C}{4} (2 + m_a \cdot (\sin(\omega t_1) + \sin(\omega t_2))) \quad (9)$$

Because m_a and T_C set values through digital logic, T is the value that can be calculated during control, t_{on} can be derived through this calculation method. However, knowing t_1 and t_2 values at each moment makes it difficult to calculate t_{on} .

As it is difficult to calculate t_{on} through the natural sampling method, using the characteristic of digital logic, the calculation method of the symmetric sampling method was used. This method can be applied when the triangular wave used as the carrier wave is symmetric. If the triangular wave is asymmetric, the error of t_{on} obtained will increase [20]. This system, which makes triangular waves through digital logic, has high reliability that triangular waves are symmetric. If t_{on} is obtained through the symmetric sampling method, it is as follows:

$$\frac{T_C}{t_{on}} = \frac{2}{1 + m_a \cdot \sin(\omega t_D)} \quad (10)$$

$$\frac{t_{on}}{2} = t_{on1} = t_{on2} \quad (11)$$

By rearranging this, the following equation can be obtained [4].

$$t_{on} = \frac{T_C}{2} \left(1 + m_a \cdot \sin\left((2n - 1) \frac{\pi}{N} \right) \right) \quad (12)$$

Where $n = 1, 2, \dots, N$, $N = m_f = \frac{f_c}{f_f}$. Another equation of t_{on} can be obtained through this calculation. As the equation shows, t_{on} can be easily obtained because the variables from the symmetric sampling method are in all known situations. In the equation, t_{on} is in the form of a sine function, which is periodic for T and has $\frac{T_C}{2}$ as the center value.

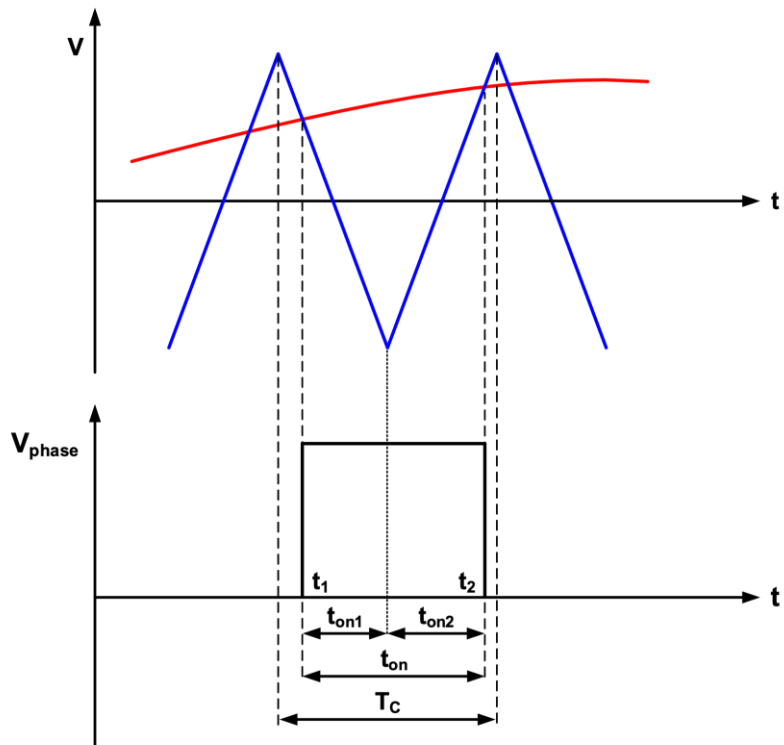


Fig. 2.1 ON pulse of phase voltage in natural sampling method.

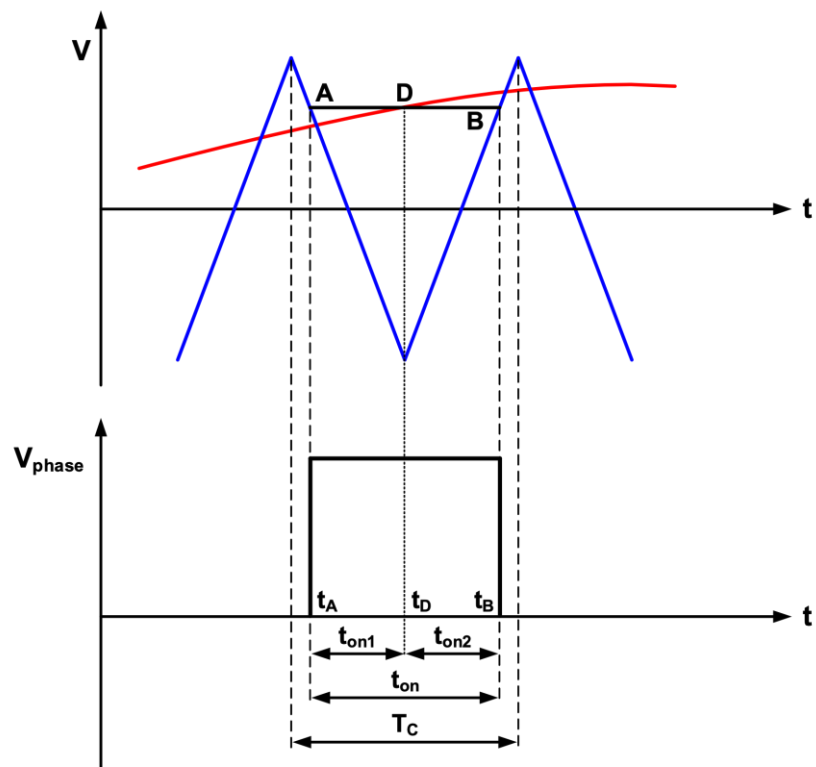


Fig. 2.2 ON pulse of phase voltage in symmetric regular sampling method.

If the equation of t_{on} obtained from the symmetric sampling method is established in the actual situation, the periodic signal can be obtained from the comparison of t_{on} and $\frac{T_c}{2}$. t_{on} obtained through the RTL simulation has the same maximum, minimum, and periodic values as the theoretical t_{on} . However, since the sinewave and triangular wave created through digital logic are composed of steps, there is a short overlap during the process of comparing the sinewave and the triangular wave. This short overlap creates the ON pulse of SPWM control for a short period of time, which makes the t_{on} value momentarily close to zero. This section makes noise in making virtual hall sensor signals, and this noise momentarily causes an error in the rotating step, making abnormal operation on sensor-less control. In the sensor-less control, the noise should be eliminated for normal operation, and the section where t_{on} becomes instantaneous zero can be eliminated by adjusting the dead-time section in dead-time control. The graph of t_{on} obtained after dead-time control from RTL simulation is similar to the theoretical t_{on} . The t_{on} graph obtained from the RTL simulation can be compared with $\frac{T_c}{2}$ to obtain a virtual hall sensor with T as the period. Terminal voltage has three phases—U, V, W, and W—each with a phase difference of 120° . The virtual hall sensor also has a phase difference of 120° each. However, using this method to obtain a virtual hall sensor is not suitable for overmodulation controls, which requires another digital ZCP filter algorithm. Fig. 2.3 shows the working of position-sensing digital ZCP filters for bipolar SPWM control in modulation. Through the algorithm, signals to be used as virtual hall sensor signals can be obtained.

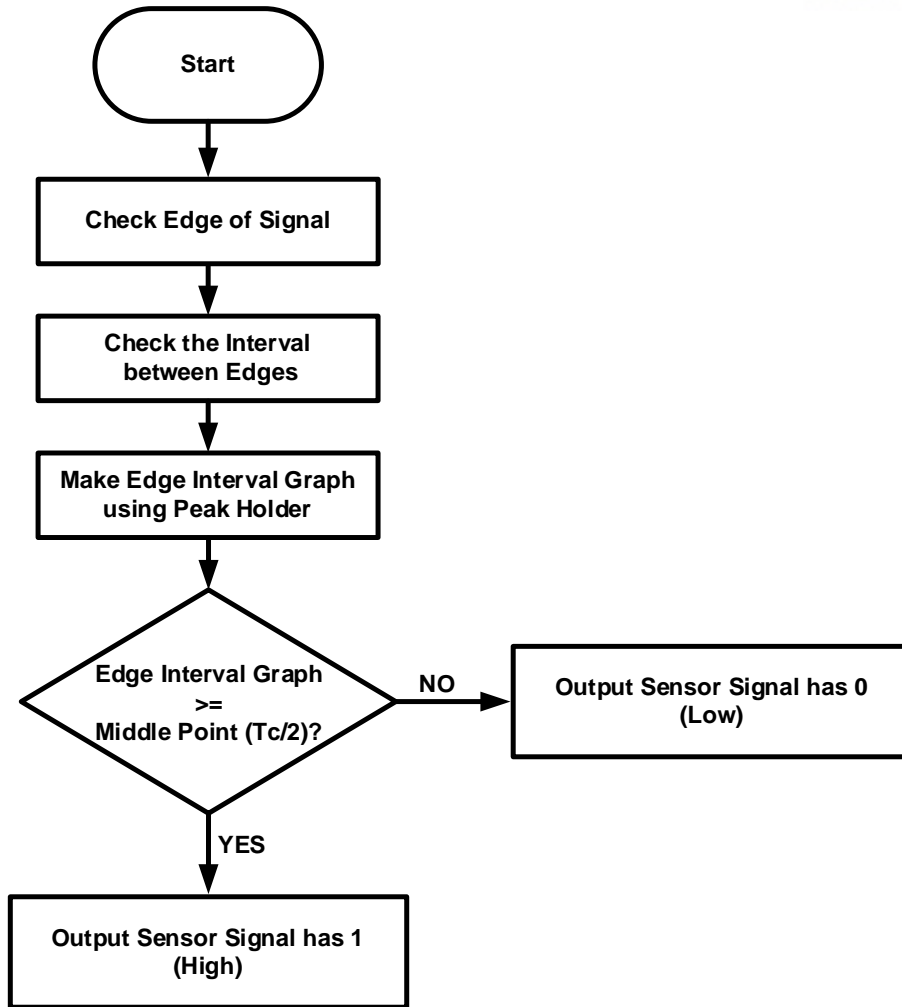


Fig. 2.3 Algorithm flowchart of position-sensing digital ZCP filter for bipolar SPWM control in modulation.

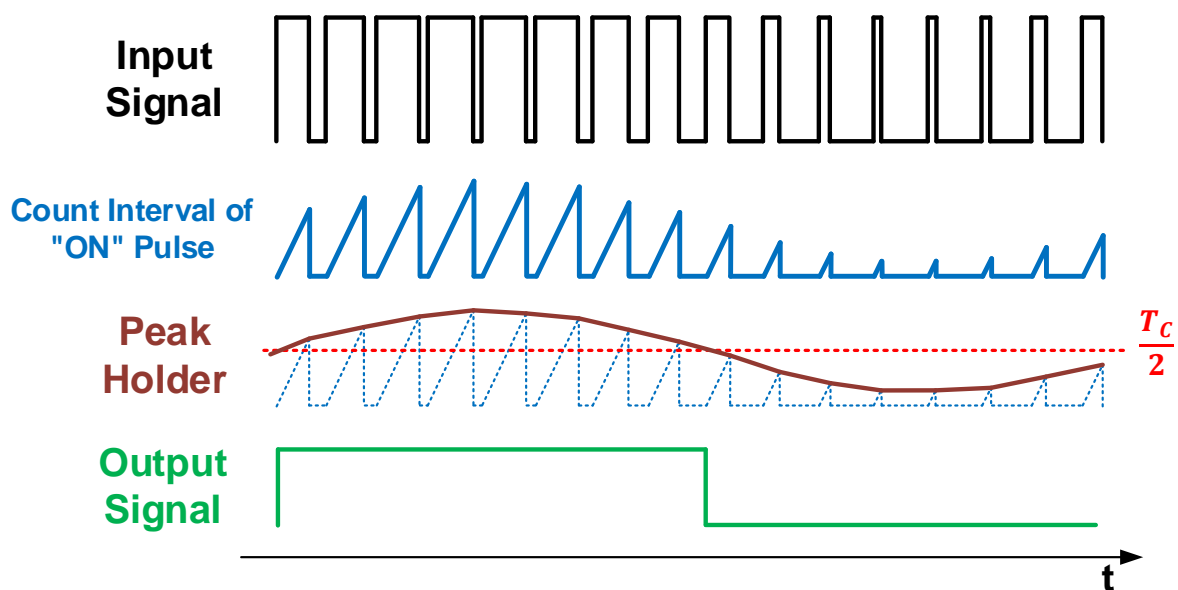


Fig. 2.4 Working of position-sensing digital ZCP filter for bipolar SPWM control in modulation.

2.2 Design of Position-sensing Digital ZCP Filter for Overmodulation and Six-step

In overmodulation, the greater the degree to which the sinewave is greater than the triangular wave, the more similar SPWM pulse becomes to the step function waveform. Also, in the case of six-step control, the terminal voltage has noise due to the commutation section where the body-diode of the MOS is turned on. In other words, the equation of t_{on} cannot be expressed in overmodulation and six-step because of such kinds of noise. Therefore, the design of the digital ZCP filter to obtain the virtual hall sensor is necessary without expressing the t_{on} equation. Therefore, a digital ZCP filter with algorithms that can eliminate noise only and produce a constant periodic signal is needed. This digital ZCP filter mainly removes the noise of the signal caused by the terminal voltage passing through the comparator.

The digital ZCP filter, which operates in overmodulation and six-step, works with the following algorithms: First, set a specific trimming value to filter. Then, measure the edge interval of the section using the counter from the rising edge of the input signal to the next rising edge. If the edge interval is greater than the filtering interval, create a detection pulse of width, such as one clock. When the detect pulse is ON, the output signal follows the current state of the input signal. Otherwise, the output signal does not change. However, the produced periodic output signal has a phase difference compared to the existing hall sensor. This phase difference must be compensated to be used as a virtual hall sensor. The step of periodic output signals should be changed through step control to match the step with the existing hall sensors to compensate this phase difference. After matching the step, change the output signal to have the same signal as the existing hall sensor by giving a delay as much as the trimming interval adjusted from the trimming value. Virtual hall sensor signals created through these algorithms replace position data provided by the hall sensors, which enables sensor-less control.

Fig. 2.4 represents the algorithm flowchart of digital ZCP filter for bipolar SPWM control in overmodulation. Fig. 2.5 shows the operation of the flowchart of Fig. 2.4. By following this flowchart, noise with frequencies above a certain frequency can be removed or ignored.

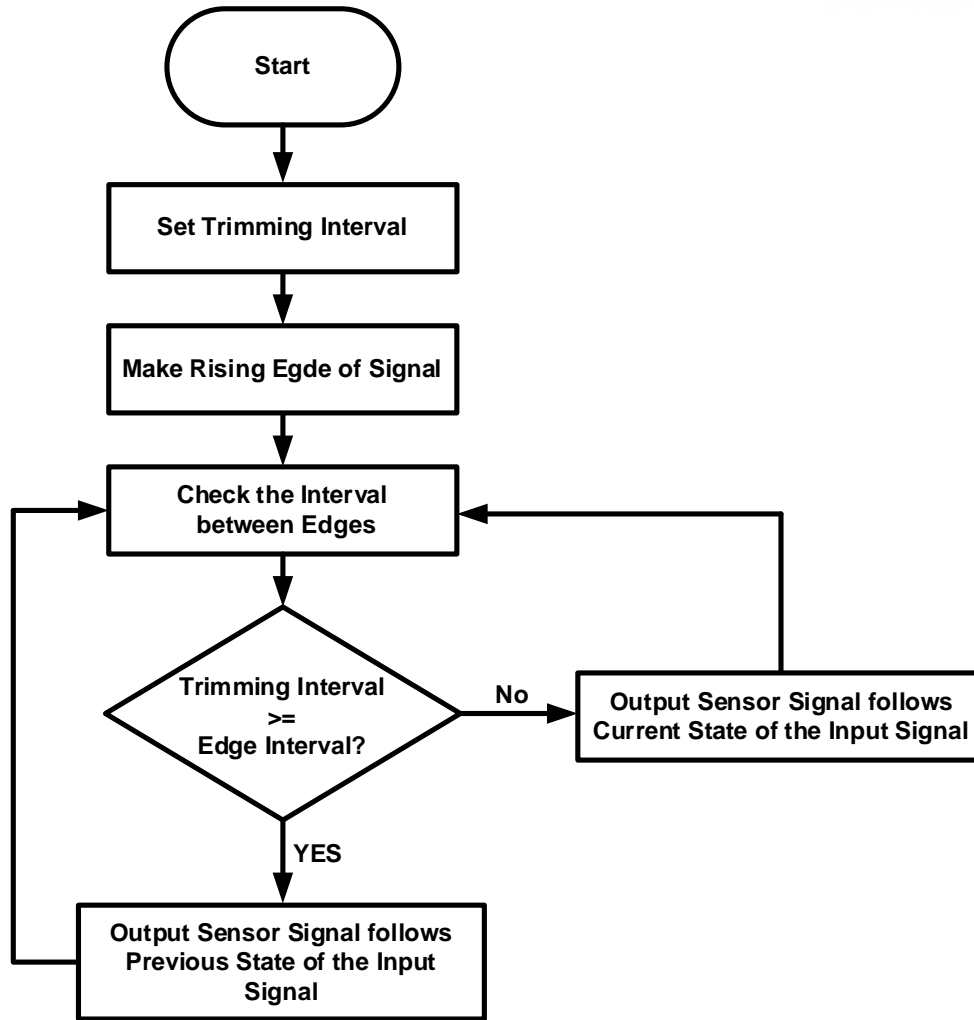


Fig. 2.5 Algorithm flowchart of position-sensing digital ZCP filter for bipolar SPWM control in overmodulation.

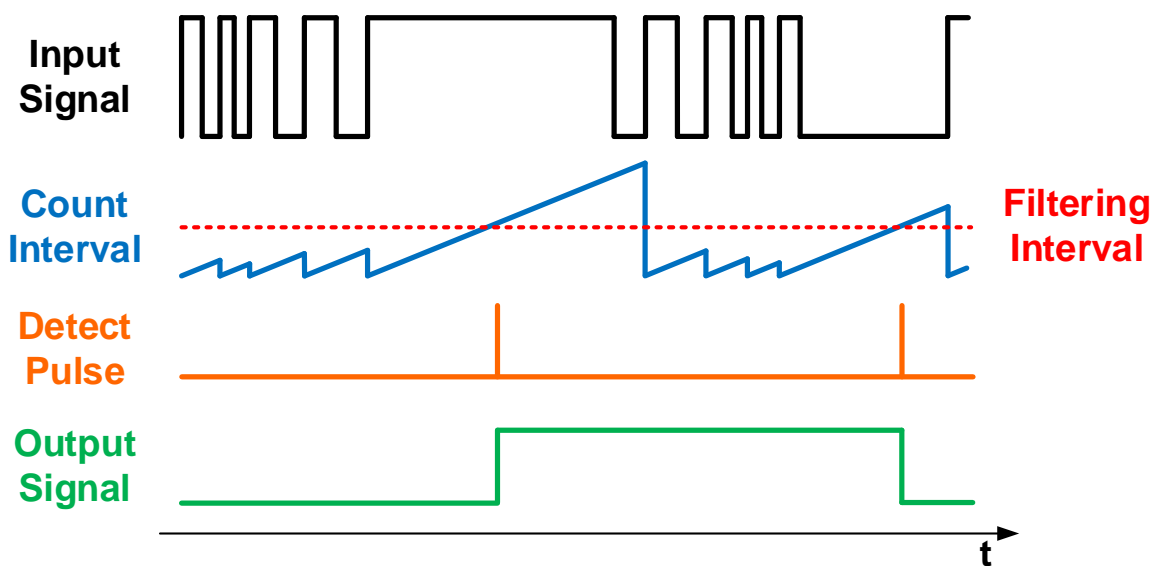


Fig. 2.6 Working of position-sensing digital ZCP filter for bipolar SPWM control in overmodulation.

2.3 Schematic of Position-sensing Digital ZCP Filter

Fig. 2.6 shows schematic of position-sensing digital ZCP filter. The schematic is created by using Verilog HDL. The role of each part is expressed related with Fig. 2.3 and Fig. 2.5.

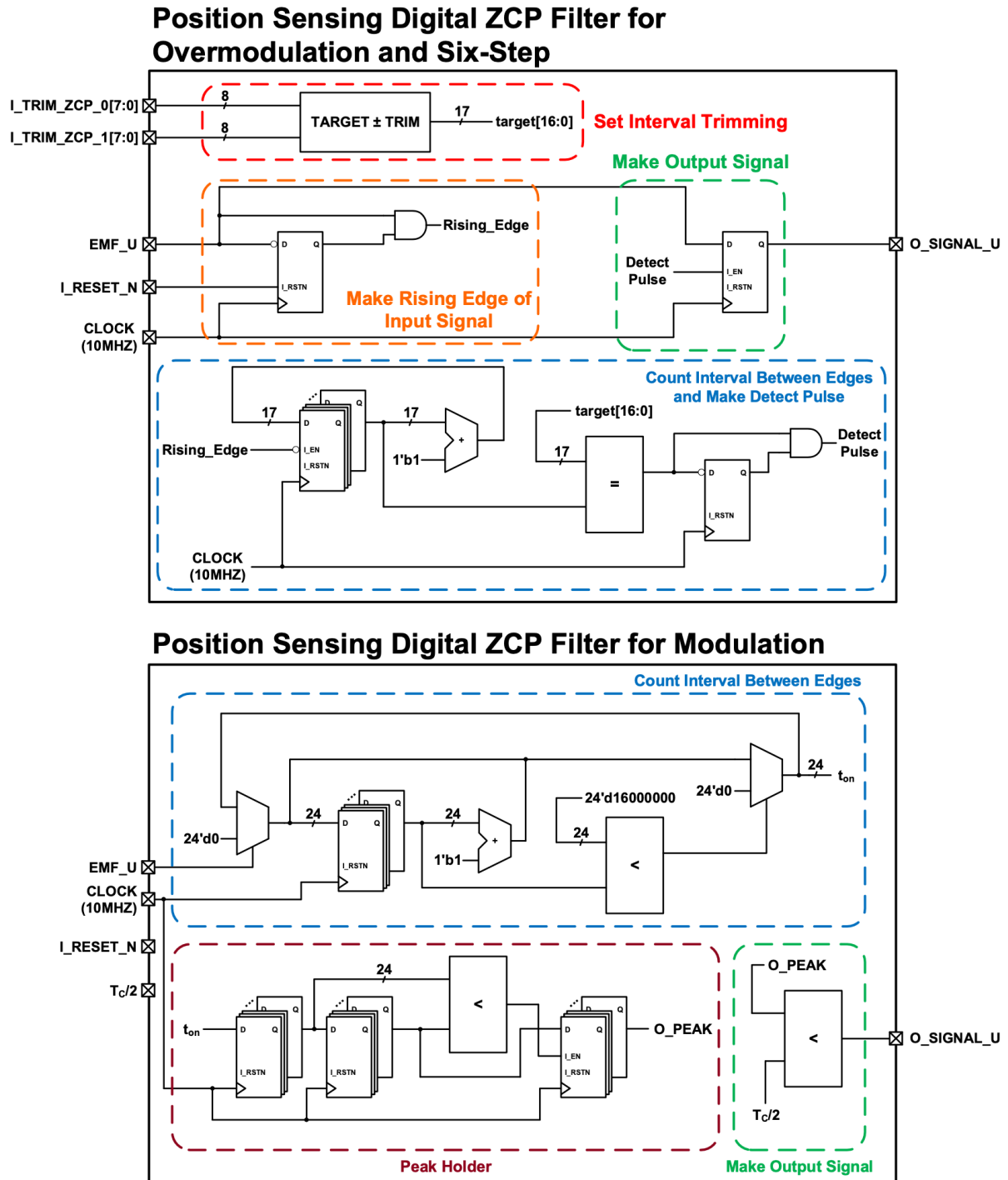


Fig. 2.7 Schematic of position-sensing digital ZCP filter.

2.4 Design of Slow Start-up Initial Driving

In sensor-less control, start-up is one of the major problems which are mostly based on back-EMF estimation techniques. The main reason is that the back-EMF voltage cannot be seen at standstill. To solve the start-up problem, an open-loop start-up is utilized in [21]. However, a temporary reverse rotation or start-up failure may occur due to unknown load characteristics and no initial rotor position information [22].

Another solution is to pre-align the rotor to the specified position by exciting any two phases of the motor for a fixed time [23]. However, during the pre-alignment, a reverse rotation or even a temporary vibration may occur. In addition, the pre-alignment may fail due to a large static friction [22]. To solve these start-up problems, many initial driving methods are proposed. Among them, methods of estimating initial rotor position were proposed. Most popular techniques to estimate the rotor position are based on the inductance variation, varying with the rotor position, which arises from the saturation effect of the stator iron core due to the permanent magnet [24]–[28]. However, such initial position-estimating methods require additional elements (e.g., current sensor, high-resolution ADC, or voltage detector). This thesis designs a PWM open-loop slow start-up initial driving algorithm. The proposed open-loop start-up consists of 2 stages: the alignment stage and the acceleration stage.

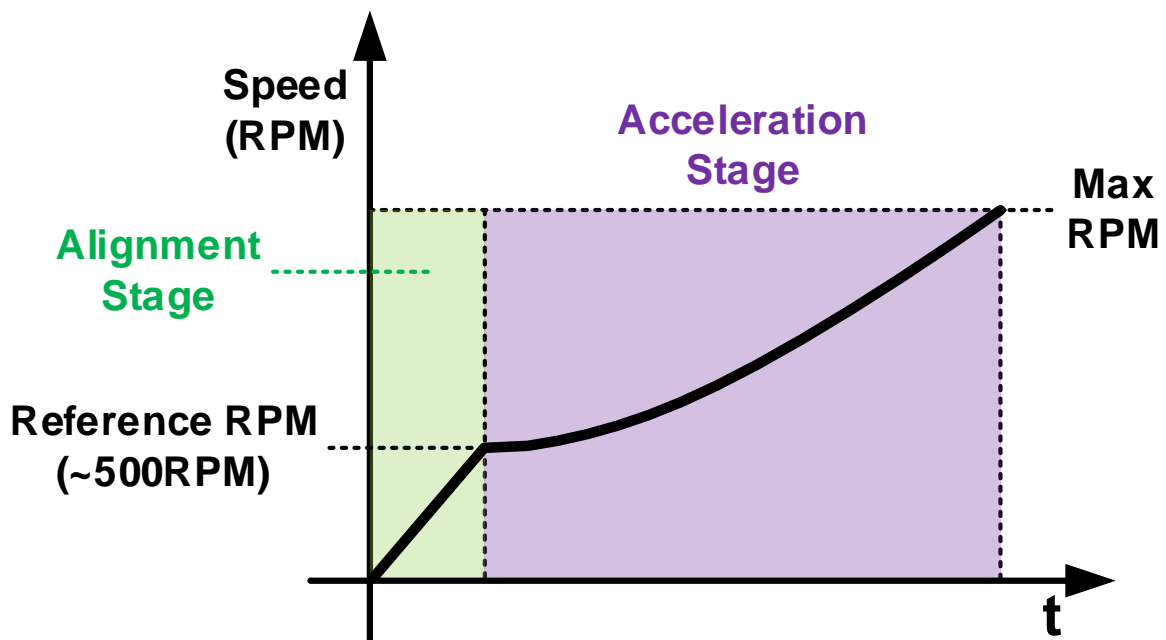


Fig. 2.8 Overall operation and speed curve of proposed initial driving.

2.4.1 Initial Driving 1st Stage: Alignment Stage

In open-loop start-up, the alignment stage should be preceded. Since the initial position of the rotor is unknown when starting the BLDC motor from a standstill, the 3-phase-inverter switches cannot be operated normally following the position of the rotor. Therefore, align the rotor to a specific position at first in the initial driving. However, in this process, the rotor can momentarily rotate rapidly or fluctuate in a moment in alignment, causing damage to the motor. It can also create problem in the following accelerating process.

The rotor is rotated by the magnetic force between rotor and magnetic field of stator. As the rotor's magnetic force cannot be changed, rotation can be controlled by changing the stator's magnetic field intensity. The equation of magnetic field intensity can be expressed as equation (13).

$$B = N \frac{\mu_0 I}{2\pi r} \quad (13)$$

Where N is the number of loop in coil, μ_0 is the permeability of free space, r is the radius of the coil, and I is the current flow in coil. As N , μ_0 , and $2\pi r$ is own characteristic of coil, only I can change the magnetic field intensity. During alignment stage, in order to align the rotor to a specific position, turn on the certain switches in 3-phase-inverter. In this working, the current that flows in the coil can be expressed as equation (14).

$$I_{coil} \approx \frac{V_{phase}}{R_{coil}} \approx \frac{V_{BAT}}{R_{coil}} \quad (14)$$

Where I_{coil} is the current flows in coil, and R_{coil} is the resistance of coil. R_{coil} can be expressed as equation (15).

$$R_{coil} \approx \rho \frac{L_{coil}}{A_{coil}} \quad (15)$$

Where ρ is metal resistivity, e.g., $1.7 \times 10^{-8} (ohm/m)$ for copper, and A_{coil} is cross-sectional area of the coil wire. Through equation (14) and (15), when the rotor is aligned to a specific position, it can be inferred that the current flowing through the coil suddenly increases.

The magnetic field intensity is stronger than the situation that the switches are turned off, which leads the magnetic field to suddenly pull or push the rotor, causing sudden fluctuations. For this reason, magnetic field intensity should become stronger in linear proportion.

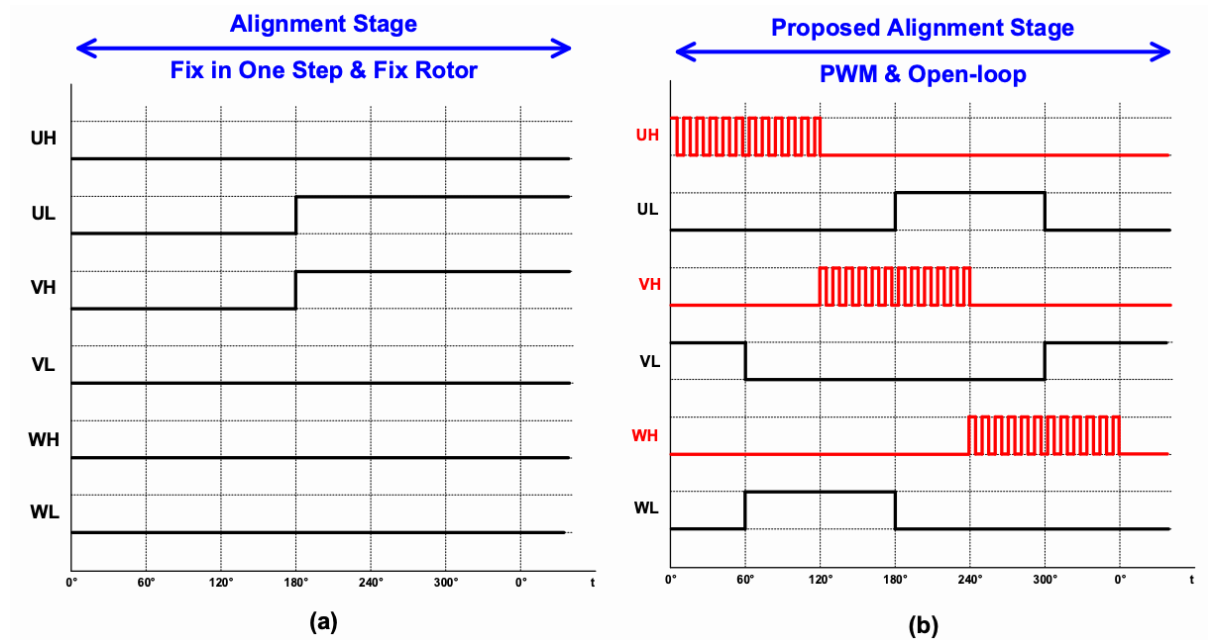


Fig. 2.9 Switching operation of the 3-phase-inverter in alignment stage. (a) is previous alignment stage operation and (b) is proposed alignment stage operation

We propose a PWM initial driving alignment to complete the operation. Unlike the conventional method, the proposed alignment stage does not turn on a specific switch but uses the PWM control to induce the rotor slowly to find its position. Fig. 2.8 shows switching operation of the 3-phase-inverter in the alignment stage. In Fig. 2.8, (a) describes a previous alignment stage operation which fixes the rotor to a specific position, while (b) is the proposed alignment stage operation. As described, in order to control magnetic field intensity, high-side switches are operated by PWM method. By turning on and off the high-side switches, an average phase current flow to the stator can be controlled. This process can lead magnetic field intensity control, and it induces and turns the rotor in a specific direction, enabling slow start-up.

PWM signal is made by comparing digital triangular wave and digital reference signal, which is used as duty ratio. The PWM signal is applied at high-side switches of 3-phase-inverter. In this case, the phase voltage of 3-phase-inverter can be expressed as equation (16).

$$V_{phase} \approx V_{BAT} \cdot Dutyratio(\%) \quad (16)$$

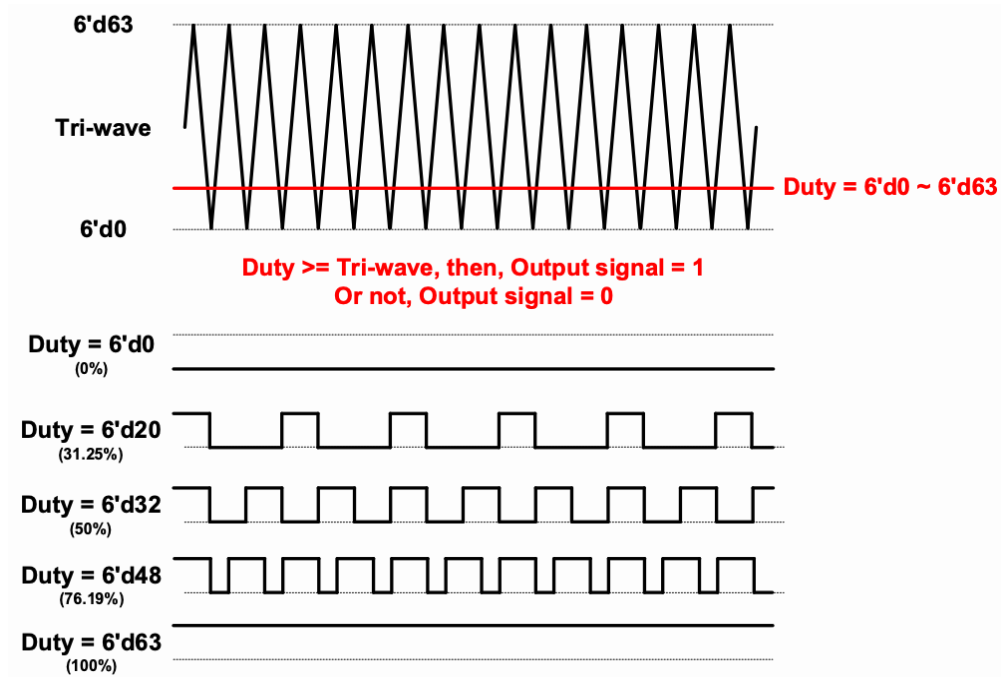


Fig. 2.10 PWM signal generating operation used in alignment stage.

The equation relationship of magnetic field intensity of coil equation (16) can be expressed as equation (17).

$$B \propto I_{coil} \approx \frac{V_{phase}}{R_{coil}} = \frac{V_{BAT}}{R_{coil}} \cdot Dutyratio(\%) \quad (17)$$

By equation (17), the magnetic field intensity can be controlled by a control duty ratio. By increasing the duty ratio linearly, the rotor speed can also be increased linearly because duty ratio and speed are in a linear relationship. The power of the motor can be expressed as equation (18).

$$power(P) = V_{phase} \cdot I_{phase} = \tau \cdot \omega_m + I^2 \cdot R + L \cdot I \cdot \left(\frac{di_{phase}}{dt} \right) \quad (18)$$

Where $\tau(N \cdot m)$ is torque and $\omega_m(rad/s)$ is angular velocity.

The equation (18) can be rearranged as equation (19).

$$V_{phase} = \frac{\tau}{I} \cdot \omega_m + I \cdot R + L \cdot \left(\frac{di_u}{dt}\right) = K_t \cdot \omega_m + I \cdot R + L \cdot \left(\frac{di_u}{dt}\right) \quad (19)$$

Where K_t is torque constant. Rearrange the equation (18) for ω_m , then equation (20) can be derived.

$$\omega_m = \frac{1}{K_t} \cdot V_{phase} - R \cdot \frac{I}{K_t} = \frac{1}{K_t} \cdot V_{phase} - R \cdot \frac{\tau}{K_t^2} \quad (20)$$

Fig 2.10 shows the graph of torque and angular speed. From the equation (20) and the equation (17), equation (21) can be derived.

$$\omega_m \propto \frac{1}{K_t} \cdot V_{phase} = \frac{V_{BAT}}{K_t} \cdot Dutyratio(\%) \quad (21)$$

As a result, both magnetic field intensity and angular velocity of motor have a linear relationship with V_{BAT} and duty ratio. By increasing the duty ratio as linearly, the magnetic field intensity and angular velocity of the motor can be increased as linearly. Therefore, this working induces the rotor to turn slowly and aligns the rotor position to the induced position.

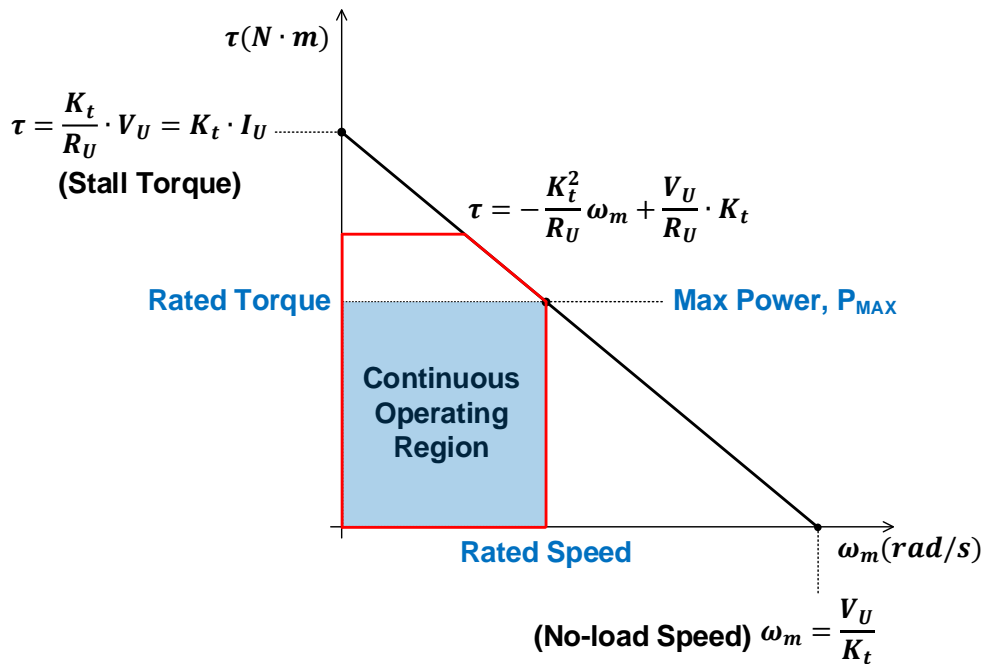


Fig. 2.11 Graph of torque and angular speed of the BLDC motor.

As shown Fig. 2.11, the specific alignment stage operation is as follows. First, set reference RPM to be operated as maximum speed in alignment stage. Second, set period of switching step depending on reference RPM. The switching step is each step that rotates at intervals of 60° . In other words, the period per one cycle of rotor is six times the switching step period. Therefore, the RPM of the motor can be expressed as equation (22).

$$RPM = \frac{60}{\text{Switchingstep} \cdot 6} = \frac{10}{\text{Switchingstep}} \quad (22)$$

Also, as motor speed is related to voltage, the RPM of the motor can be expressed as equation (23).

$$RPM = \frac{V_{BAT}}{V_{Rated}} \cdot RPM_{Rated} \cdot \text{Dutyratio}(\%) \quad (23)$$

Where V_{Rated} is rated voltage of BLDC motor, and RPM_{Rated} is rated speed (RPM) of BLDC motor.

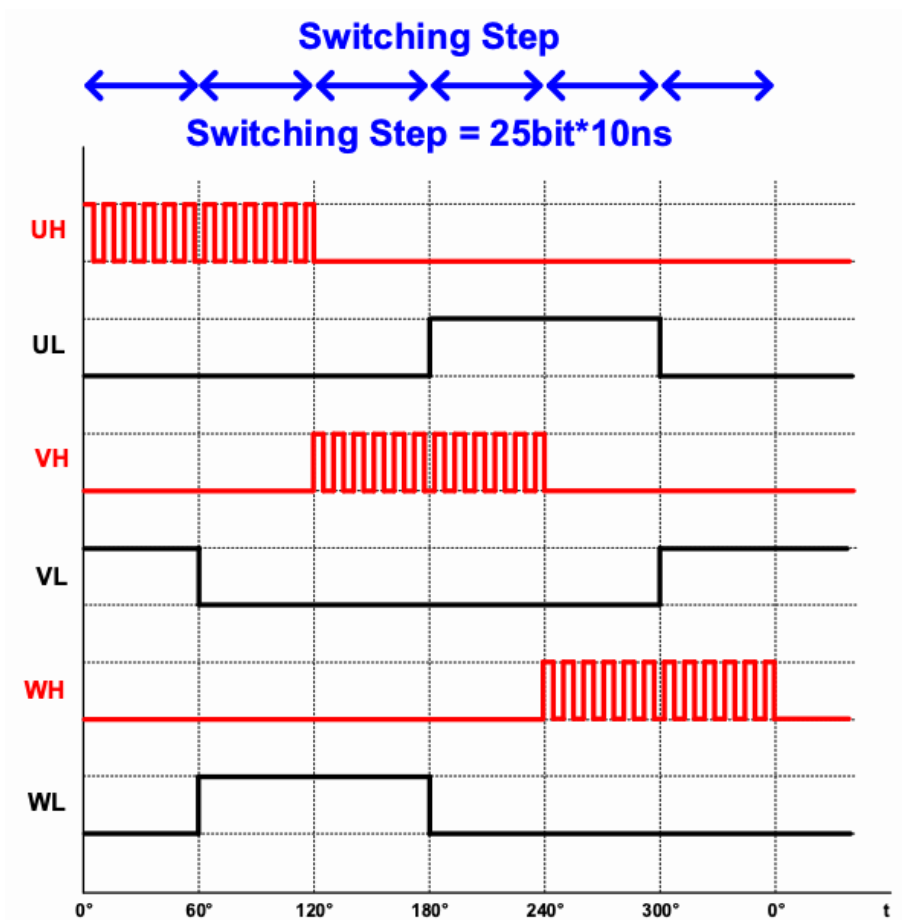


Fig. 2.12 Switching step of alignment stage.

Third, increase duty ratio linearly from 0% to 100%. This operation increases the RPM of the motor linearly according to the increase in duty ratio. In this design, duty ratio increases by 1/64 (1.5625 %) per switching step. Fig. 2.12 shows operation of increasing speed and duty in the alignment stage. According to the set reference RPM and alignment time, duty increases linearly. If the rotor starts up slowly and if the RPM of the motor reaches to the reference RPM through this process, start the acceleration stage.

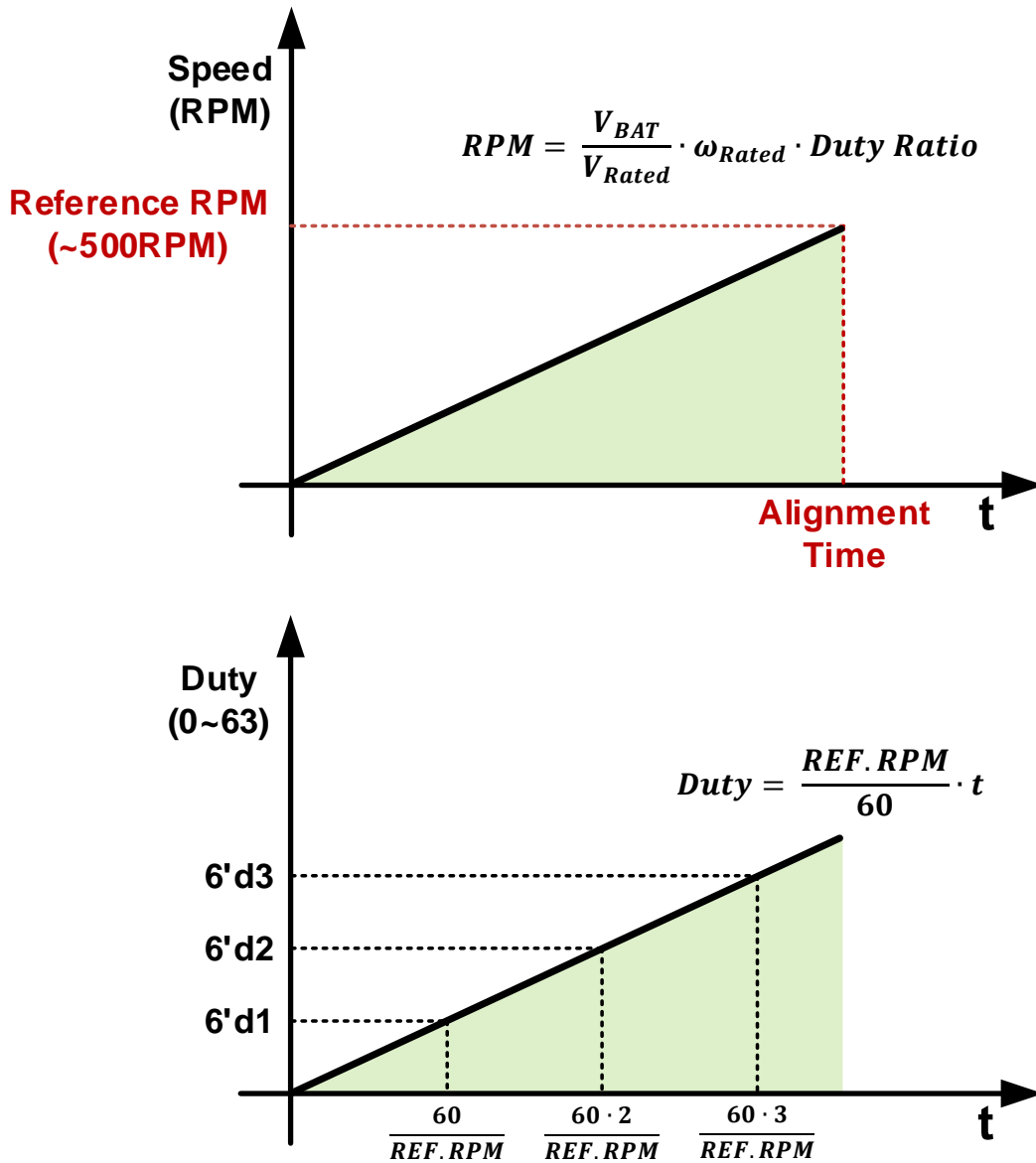


Fig. 2.13 Increase of speed and duty in the alignment stage.

2.4.2 Initial Driving 2nd Stage: Acceleration Stage

After the alignment stage, acceleration stage begins. The acceleration stage operates with a gradual increasing switching frequency of the six-step control. Similar to controlling a stepper motor, this process controls the BLDC motor as an open-loop synchronous motor. To control the rotor in the acceleration stage, the acceleration block borrows initial driving curve of Texas Instrument, TI-DRV10983 [29]. The speed equation of acceleration stage can be shown like equation (24).

$$Speed = a_1 \cdot t + \frac{1}{2} \cdot a_2 \cdot t^2 \quad (24)$$

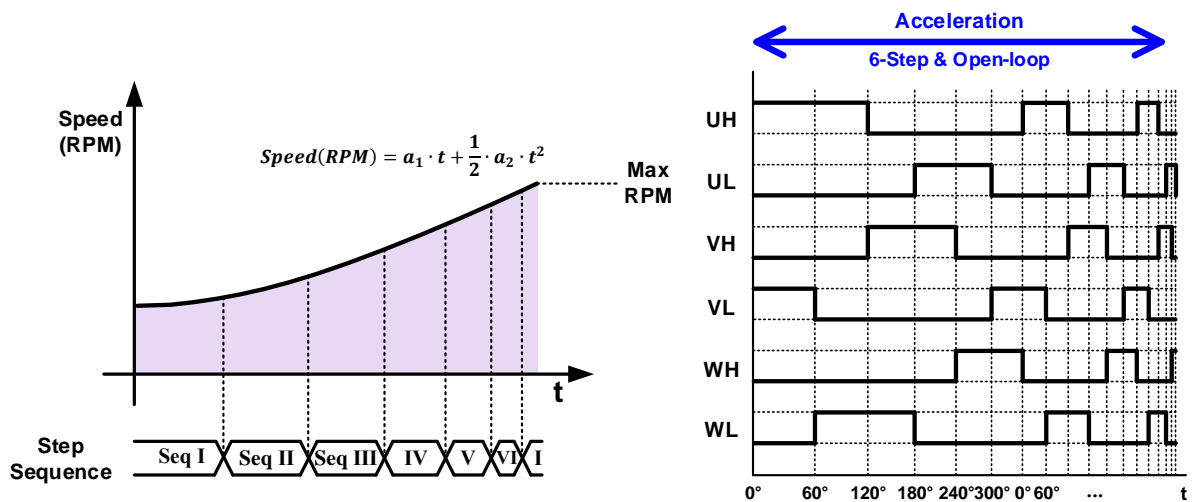


Fig. 2.14 Speed graph and step sequence in acceleration stage.

From the speed equation, as shown in Fig. 2.13, speed up the motor by gradually decreasing the step time. During the acceleration stage, the position-sensing digital ZCP filter for overmodulation and six-step obtains virtual hall sensors from the U, V, W phase voltages. After obtaining the virtual hall sensor through the position-sensing block, check that it correctly obtains the rotor position according to the sequence of steps. If the steps are in a constant sequence, either clockwise or counterclockwise, for several laps continuously, the normal sensor-less operation begins. Afterwards, while switching the 3-phase-inverter to a constant frequency, V_{BAT} is changed and the speed of the motor is controlled.

2.4.3 Initial Driving TOP Block Diagram

The initial driving TOP Block is shown in Fig 2.14. Each of the alignment stage blocks and acceleration stage blocks produces a gate control signal that goes into the 3-phase-inverter. This signal is selected through the gate control signal MUX. From the acceleration stage, virtual hall sensor signals are created using a position-sensing digital ZCP filter for overmodulation & six-step. If the step of virtual hall sensor signals is consistently matched through the checking step block, normal operation starts. The initial driving block was also made in Verilog HDL.

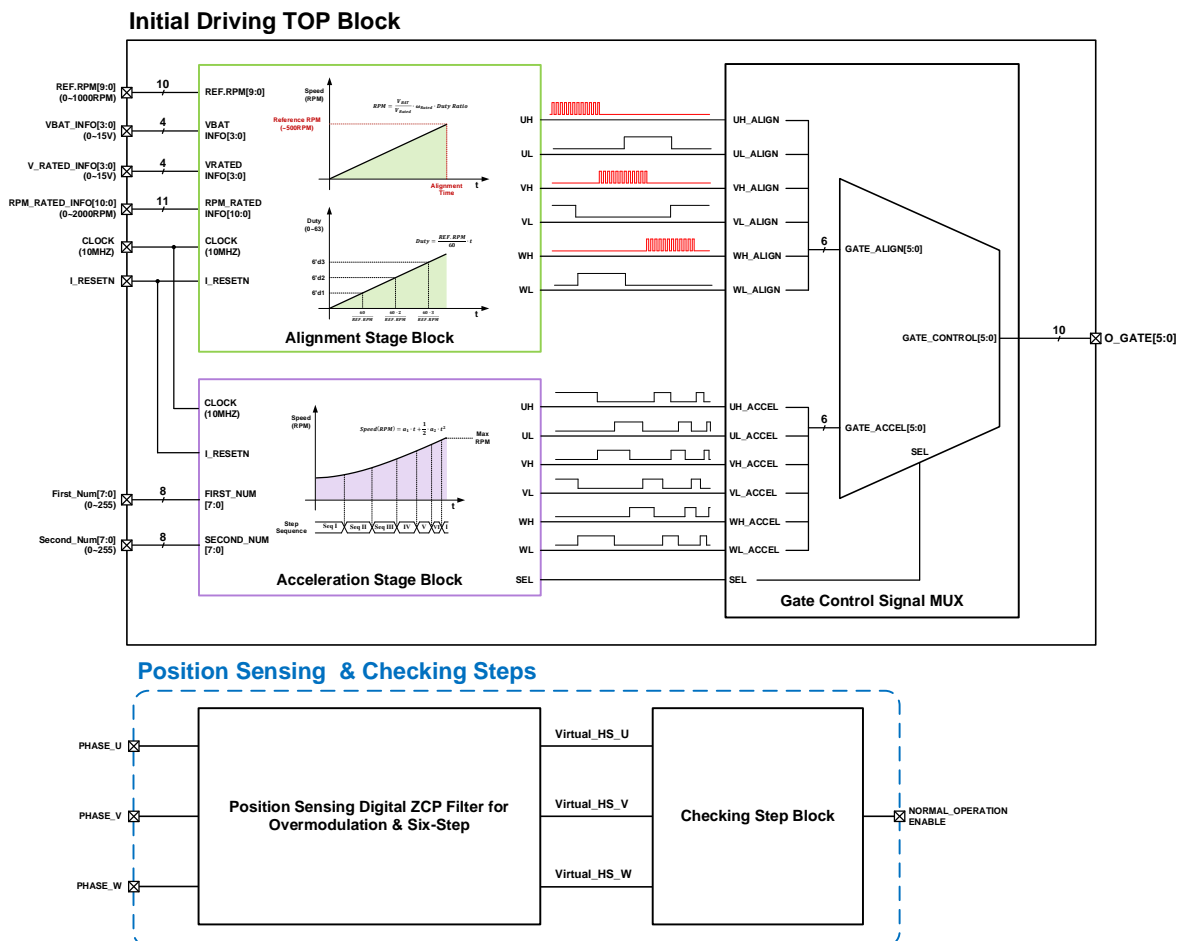


Fig. 2.15 Initial driving TOP block diagram.

2.5 TOP Block Diagram of SPWM Sensor-less BLDC Controller

Fig. 2.15 shows SPWM sensor-less BLDC motor controller TOP block diagram. It consists of the circuits described and suggested above. Through the mode selection block, the TOP block can be operated with a desired control (i.e., six-step control, overmodulation SPWM control or modulation SPWM control). By distinguishing between initial driving and normal operation through gate signal MUX, both the initial driving TOP block and the bipolar SPWM BLDC motor controller generate 3-phase-inverter gate control signals as output signals. To control the position-sensing digital ZCP filter, bipolar SPWM BLDC motor controller, and trimming value used in the initial driving block, a separate internal register control block is designed. All blocks, including the register block that controls the trimming value and gate signal MUX, are created using Verilog HDL, as is the TOP block including the register control block and gate signal MUX.

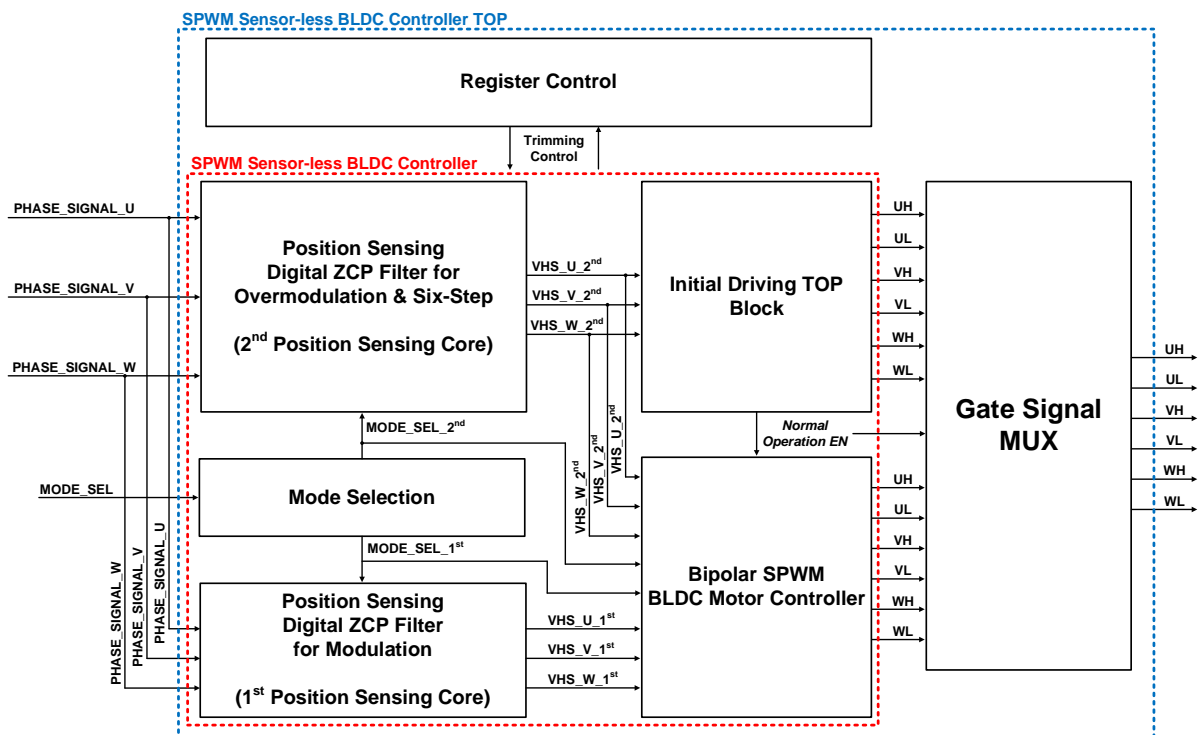


Fig. 2.16 SPWM sensor-less BLDC motor controller TOP block diagram.

3. Simulation and Experiment Results

3.1 Simulation Results

To check the operation of the RTL code, after making a testbench with Verilog HDL, designed blocks are checked by using Questa's Modelsim. The Fig. 3.1 shows the simulation result of position sensing digital ZCP filter for modulation. The ON pulse peak holder graph shows the sinusoidal wave form following Fig. 2.4. The output signals of Fig. 2.4 which are made from comparing ON pulse peak holder graph and $\frac{T_C}{2}$ are also shown in Fig. 3.1 From Fig. 3.1, it can be seen that the virtual hall sensor signals are made from the ON pulse peak holder graph. Also, it follows the steps of original hall sensor signals. As the steps The steps of the virtual hall sensors coincide with the steps of the original hall sensors, and the delay difference between the original and virtual signals is within 5% of the signal period. This means that the signals generated by position sensing digital ZCP filter for modulation can be used for sensor-less driving.

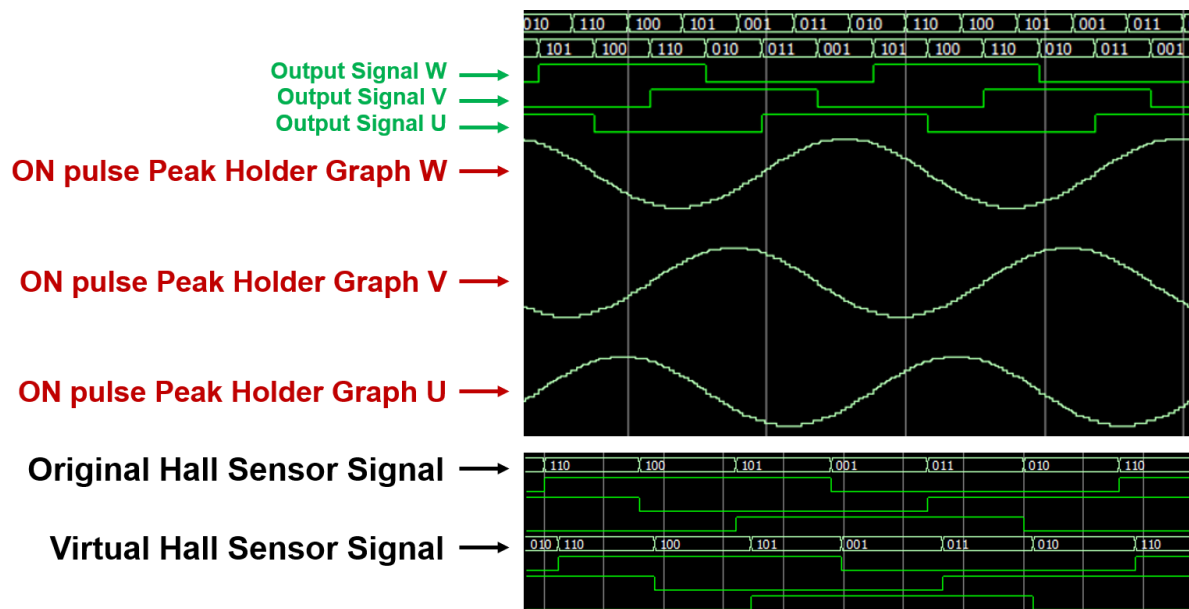


Fig. 3.1 Simulation of position sensing digital ZCP filter for modulation.

The Fig. 3.2 shows the simulation result of position sensing digital ZCP filter for overmodulation. Following Fig. 2.6, the output signals are made from the phase signal which can be seen in Fig. 3.2. From Fig. 3.2, it can be seen that the virtual hall sensor signals are made from the count interval graph. By comparing count interval and filtering interval, detect pulse is on, and the output signal follows the current state of phase signal. Also, steps of virtual hall sensor signal follows the steps of original hall sensor signals. It also shows that the signals generated by position sensing digital ZCP filter for overmodulation can be also used for sensor-less driving in SPWM overmodulation. Fig. 3.3 shows the gate signals in slow start-up alignment stage and acceleration stage. The simulation results come out as designed, and the designed circuits are verified that they actually operate normally through experiments.

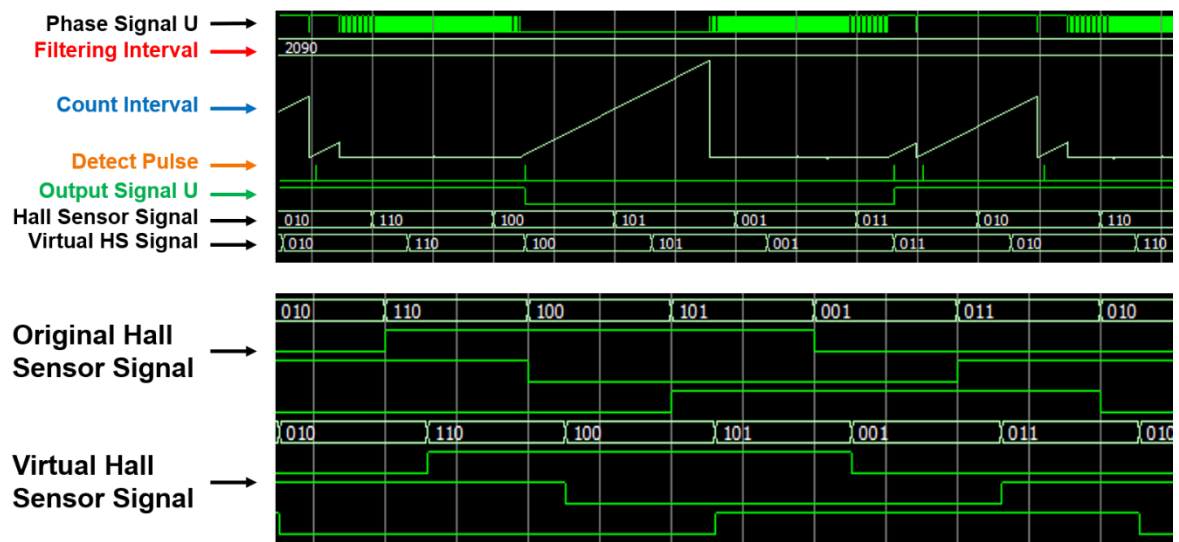


Fig. 3.2 Simulation of position sensing digital ZCP filter for overmodulation.

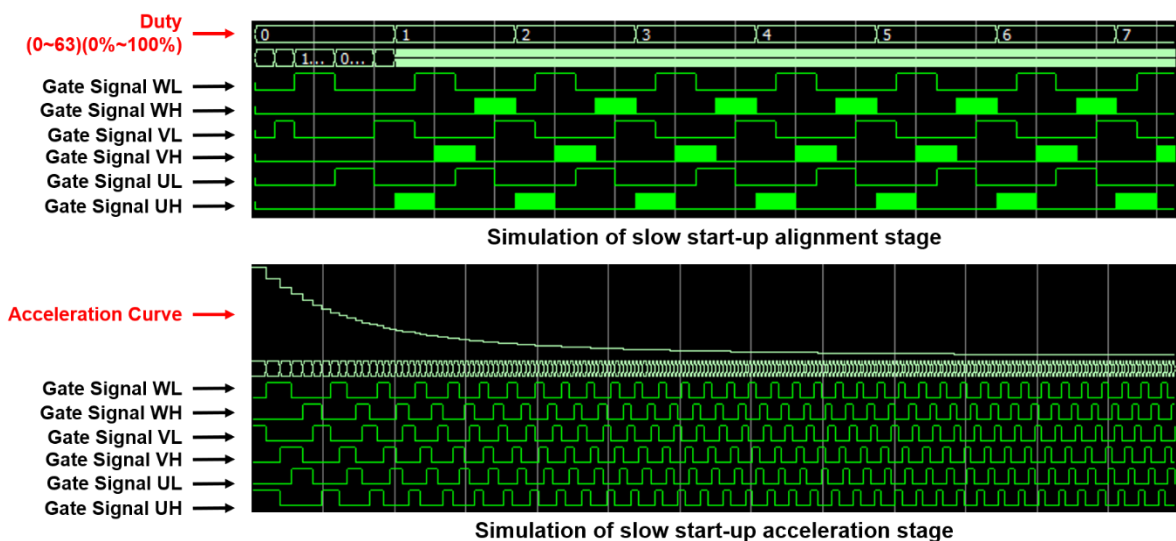


Fig. 3.3 Simulation of slow start-up alignment stage & acceleration stage.

3.2 Experiment Setup

The specification of BLDC motor used in the experiment is shown in Table. 3.1. The BLDC motor used in the experiment is BD42-I012007 from Sewoo Industrial Systems. It has a rotor of 4 poles, a rated voltage of 12V, a rated power of 7W, and a rated speed of 2400RPM. From the specification, information of rated voltage and rated speed required for initial driving can be obtained. Table. 3.2 shows the specification of 3-phase-inverter used in the experiment. The 3-phase-inverter used in the experiment is HIP2103-4DEMO2Z from Renesas. It includes pre-drivers HIP-2103 and HIP-2104 which is compatible with 3.3V or 5V logic. In order to control this 3-phase-inverter and to prevent shoot-through current, it must have a clear sleep time of at least 20us and a minimum dead-time of 200ns. Fig.3.1 and Fig.3.2 show the test board of the experiment and the block diagram of the experiment setup environment. Using a power supply and function generator, VBAT is supplied to 3-phase-inverter and 10MHZ clock is supplied to SPWM sensor-less BLDC motor.

Table. 3.1 Specification of BLDC motor (BD42) used in the experiment.

Parameters	Values
Rated voltage	12V
Rated speed	2400RPM
Rated output	7W
Rated torque	0.28 kgf-cm
Number of poles	4

Table. 3.2 Specification of 3-phase-inverter (HIP2103-4DEMO2Z) used in the experiment.

Parameters	Values
Operating voltage range	5V to 40VDC
Maximum continuous bridge current	60A (with sufficient air flow and/or heatsinking)
Minimum time for clear sleep mode	20us
Minimum dead-time	200ns
High-side input voltage	3.3V or 5V logic compatible
Low-side input voltage	3.3V or 5V logic compatible

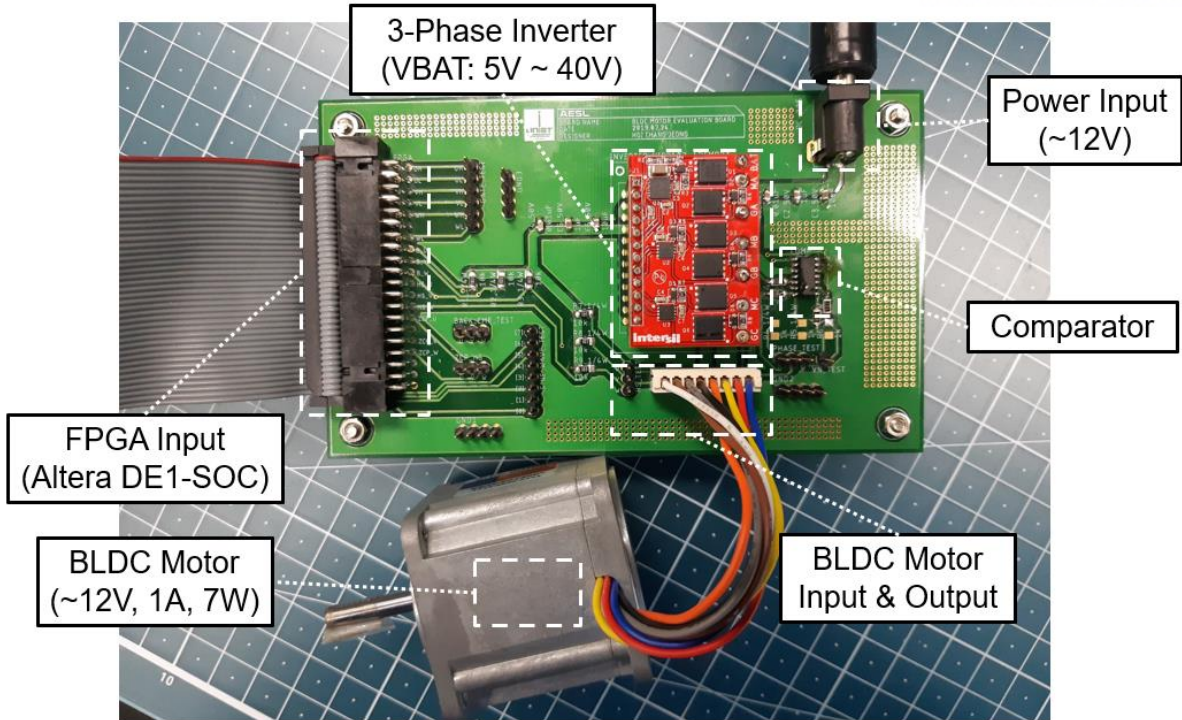


Fig. 3.4 Test board of the experiment.

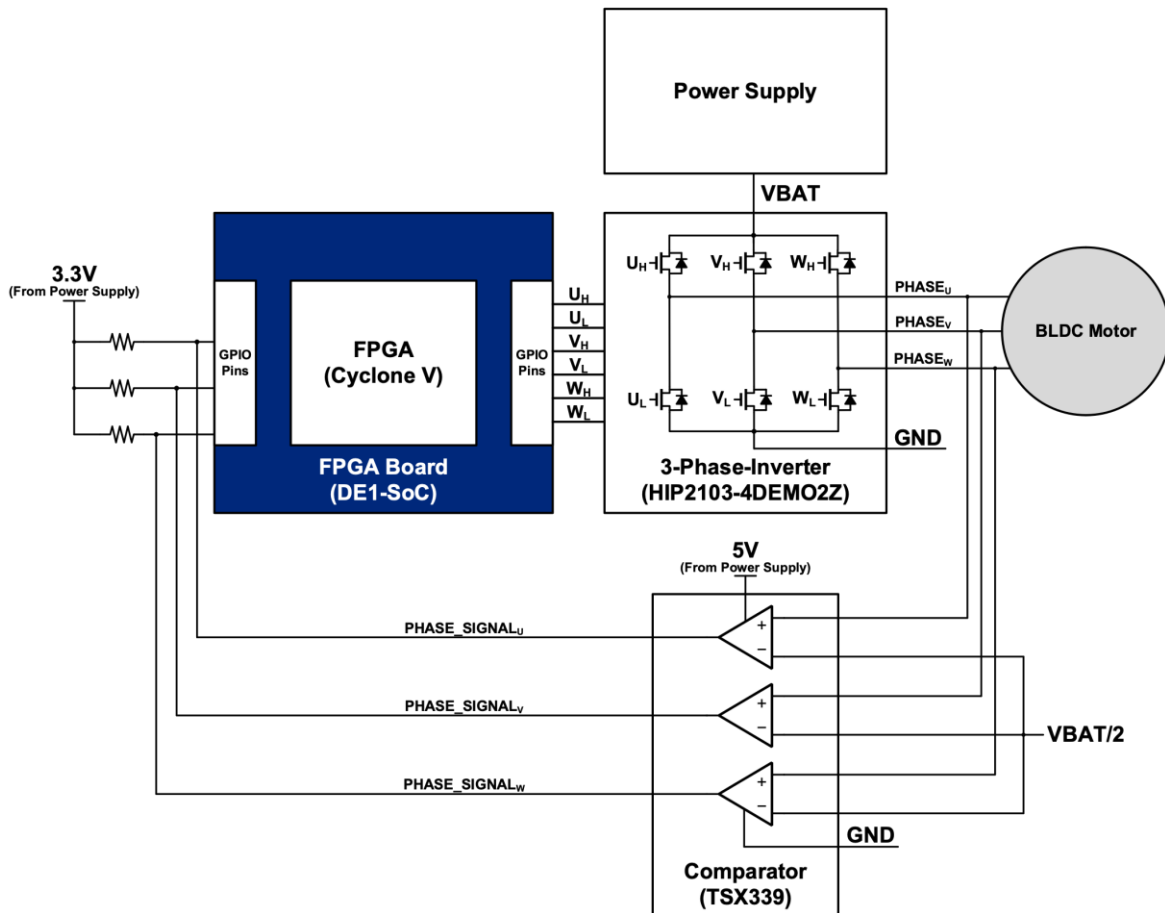
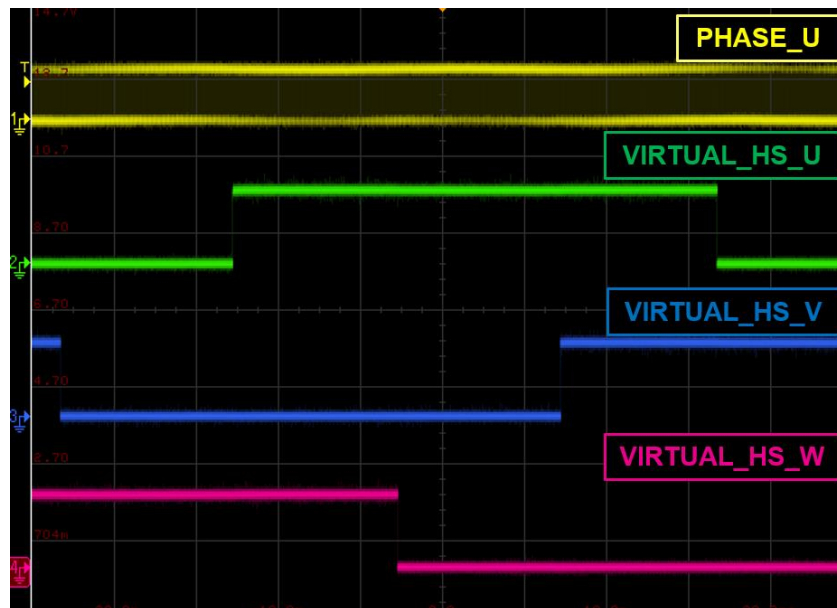


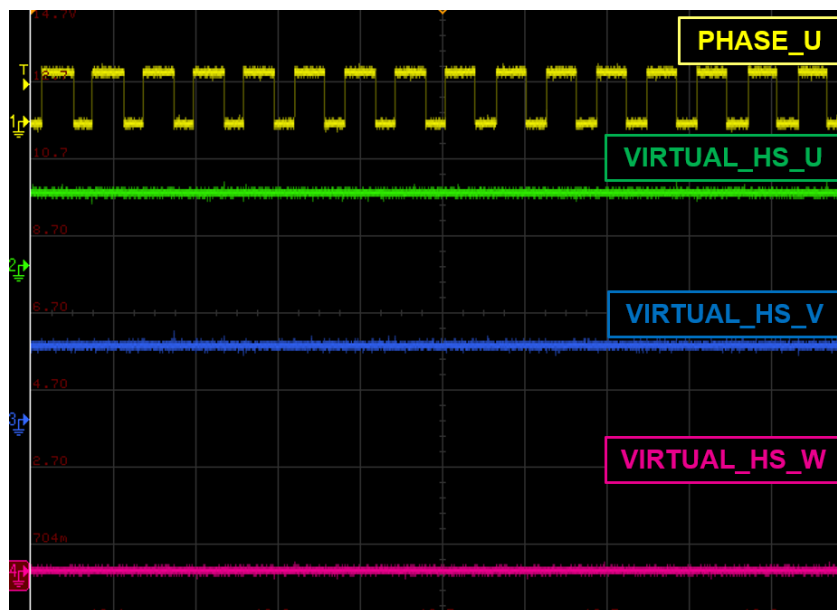
Fig. 3.5 Block diagram of experiment setup.

3.3 Experiment Results

Fig. 3.3 shows the getting virtual hall sensor signals by position-sensing digital ZCP filter for SPWM modulation control. As shown in the figure, it can be seen that the virtual hall sensor signal is created. The enlarged figure shows the phase voltage in SPWM modulation control.



(a)

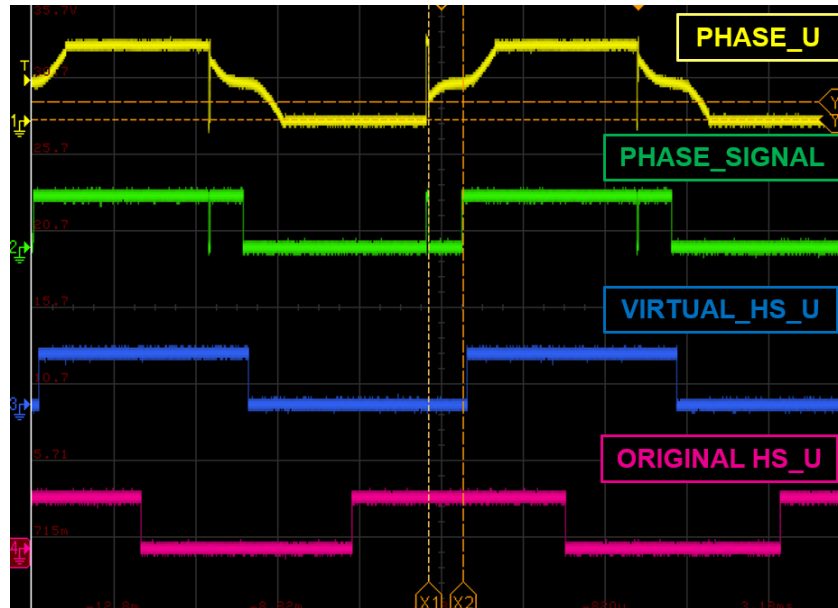


(b)

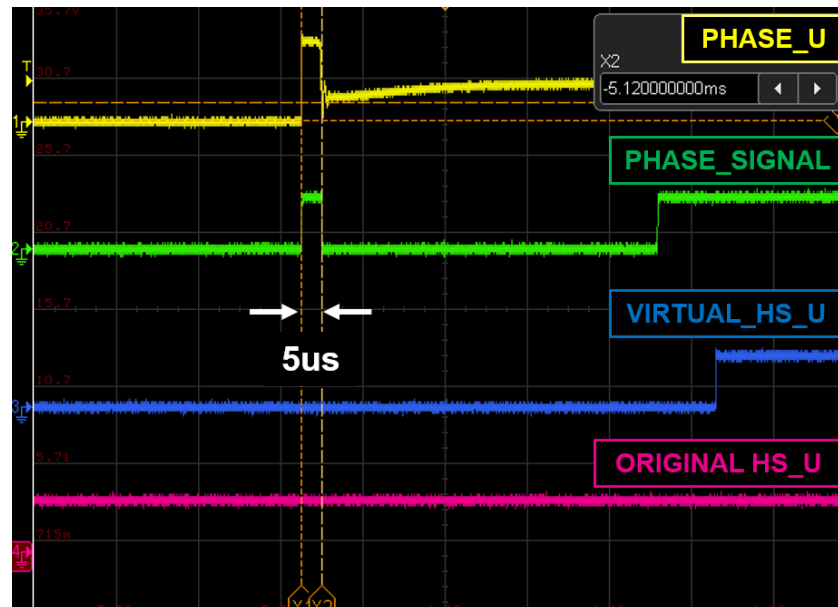
Fig. 3.6 Getting virtual hall sensor signal by position-sensing digital ZCP filter for modulation.

(a) is modulation control and (b) is enlarged figure of (a).

Fig. 3.4 shows the getting virtual hall sensor signals by position-sensing digital ZCP filter for overmodulation and six-step in six-step control. As shown in the figure, it can be seen that the virtual hall sensor signal is created using the phase signal generated from the phase voltage. The virtual hall sensor signal can be obtained by filtering the noise generated by the freewheeling diode.



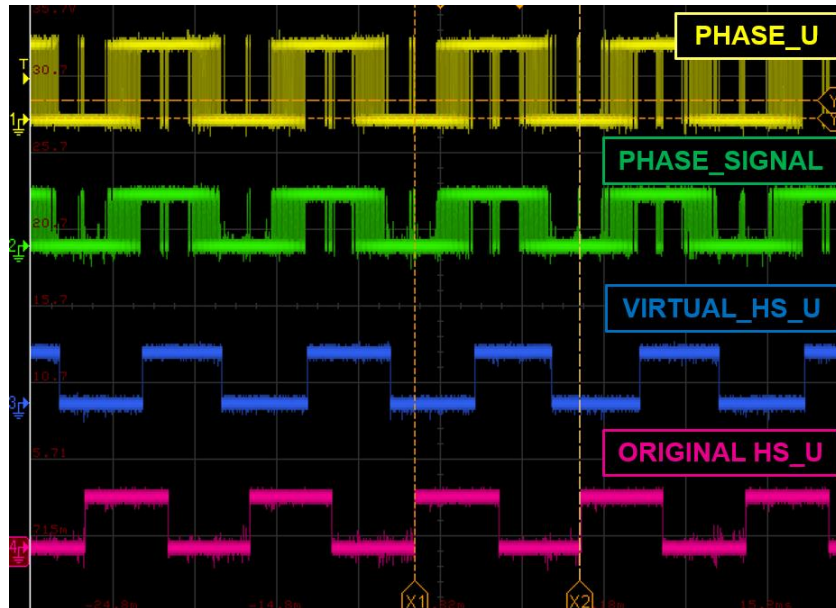
(a)



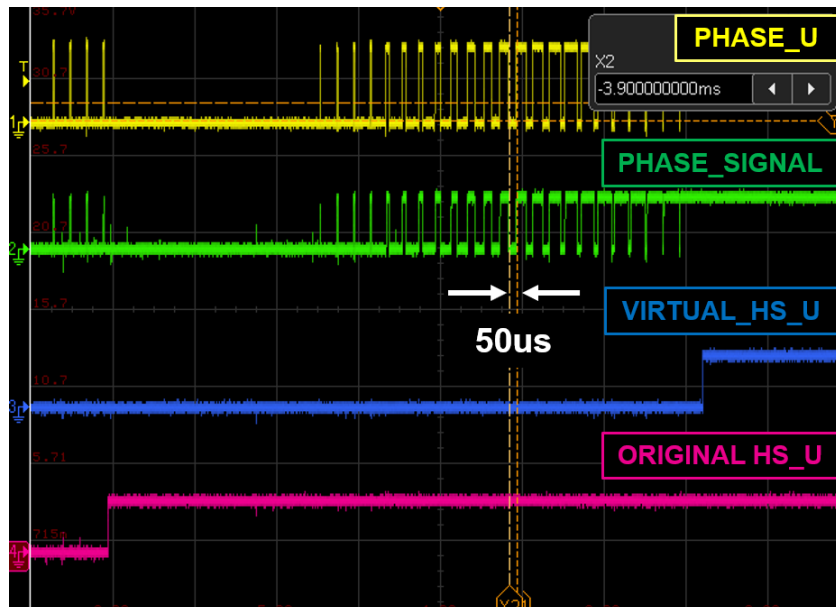
(b)

Fig. 3.7 Getting virtual hall sensor signal by position-sensing digital ZCP filter for overmodulation and six-step. (a) is six-step control and (b) is filtering interval.

Fig. 3.5 shows the getting virtual hall sensor signals by position-sensing digital ZCP filter for overmodulation and six-step in overmodulation control. As shown in the figure, virtual hall sensor signal is created using the phase signal generated from the phase voltage. Virtual hall sensor signal can be created through filtering as in six-step. Since the filtering interval differs according to the VBAT and interval of dead-time control, the trimming of the position-sensing digital ZCP filter must be adjusted.



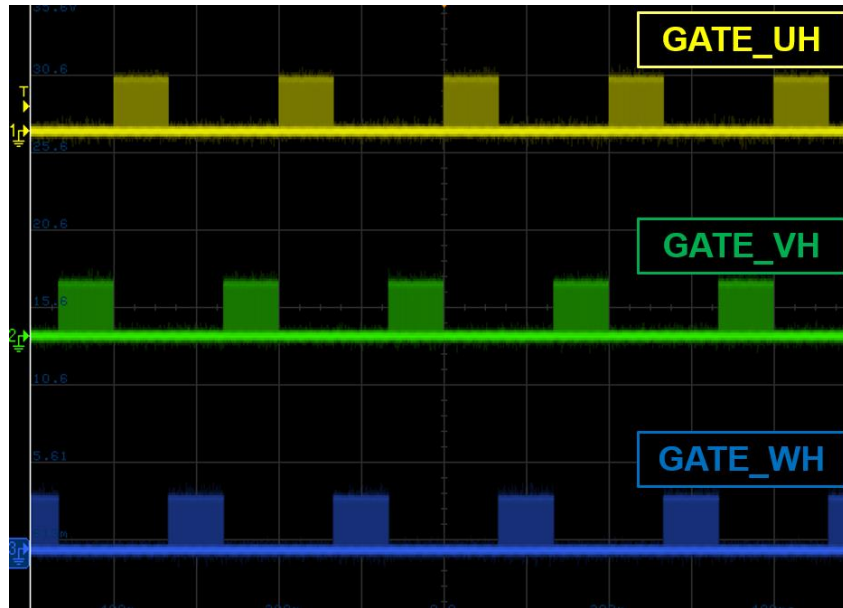
(a)



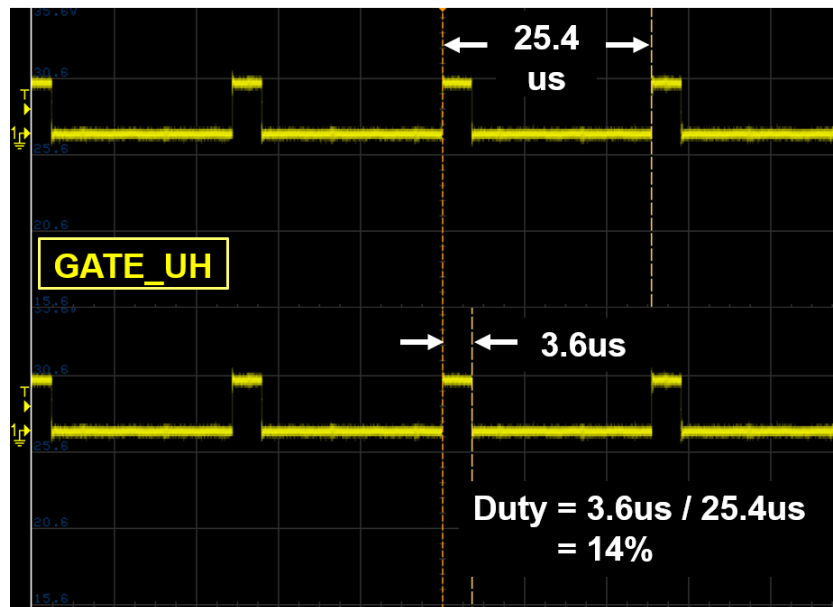
(b)

Fig. 3.8 Getting virtual hall sensor signal by position-sensing digital ZCP filter for six-step and overmodulation. (a) is overmodulation control and (b) is filtering interval.

Fig. 3.6 shows the high-side gate control signals in slow start-up initial driving. As shown in the figure, high-side gate control signals have the form of a PWM signal depending on the duty ratio. For instance, in Fig. 3.6 (b) shows PWM signal used for high-side switch of U phase and duty ratio. From these experiment results, it can be seen that the SPWM sensor-less BLDC motor controller works as designed.



(a)



(b)

Fig. 3.9 High-side gate control signals in slow start-up initial driving.
 (a) is high-side gate control signals and (b) is enlarged GATE_UH signal in (a).

4. Conclusion

This thesis presents a position-sensing ZCP filter for 3-phase sinusoidal BLDC motor controller and slow start-up initial driving, which are necessary for BLDC motor sensor-less control. The proposed position-sensing ZCP filter can determine the position of the internal rotor by generating virtual hall sensor signals from the phase voltages of a BLDC motor. The position-sensing ZCP filter consists of two cores each operating in six-step control and SPWM control. In addition, the proposed slow start-up initial driving, consisting of two stages, can prevent reverses in rotation or temporary vibration that occurs during pre-alignment. The SPWM sensor-less BLDC motor control is implemented through the above proposed circuit and algorithm.

5. Future Works

With the proposed SPWM sensor-less BLDC motor controller, additional PID controller about position-sensing ZCP filter is necessary for making more accurate virtual hall sensor signals. First, a complementary circuit is required according to sudden torque or speed changes. Sensor-less control works based on a certain speed of 1000-2000rpm or more because of virtual hall sensor signals. In addition, the sudden application of a large load to the BLDC motor will impair rotation, making virtual hall sensor signals impossible. To solve these problems, an additional complementary circuit is needed to create virtual hall sensor signals according to variables of speed and torque through a PID controller. In addition, it is necessary to prepare for situations in which the torque changes due to a sudden large load, and the virtual hall sensor signals generated based on the phase voltage will not appear. To this end, sensor-less control must be compensated by adding a method to create virtual hall sensor signals through phase current sensing. Second, it is necessary to automatically set the trimming value used in the digital ZCP filter for overmodulation. The trimming value used as an input in the digital ZCP filter for overmodulation is used to eliminate noise above a certain frequency of the phase voltage, and the location of the virtual hall sensor signals varies according to the trimming value. Also, since the frequency of the phase voltage noise varies according to the speed of the BLDC motor, the trimming value must be changed according to the speed. It is necessary to control for the change in the trimming value with a PID controller dedicated to ZCP filter.

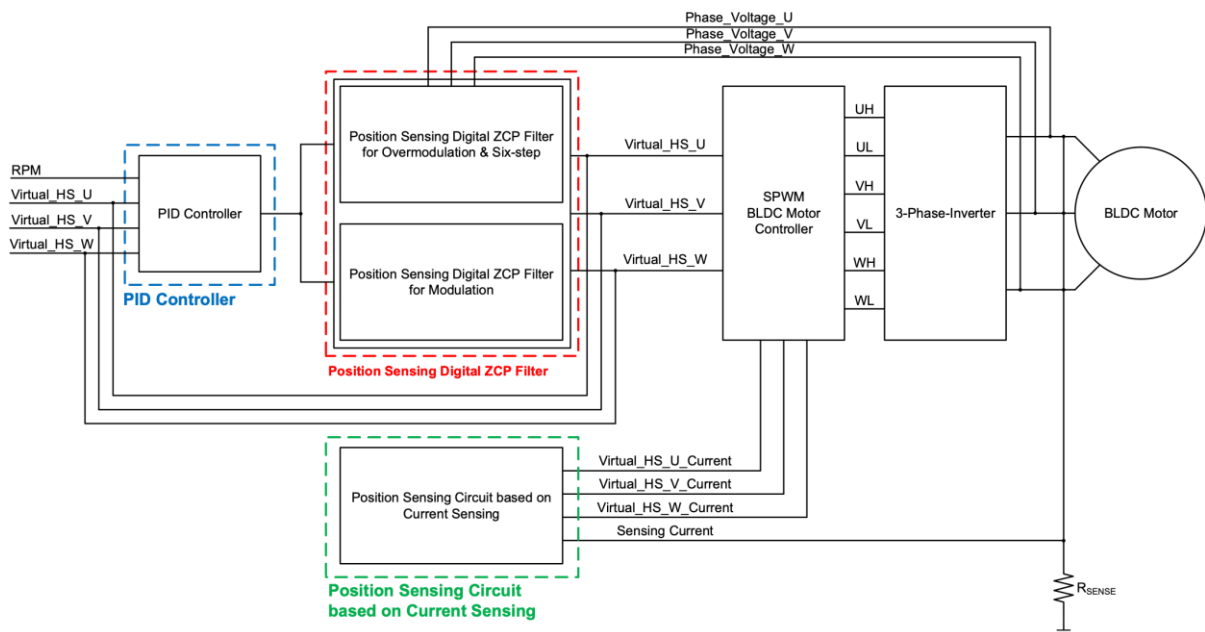


Fig. 5.1 Proposed SPWM sensor-less BLDC controller applying with PID controller.

REFERENCES

- [1] Bimal K. Bose, “Modern Power Electronics and AC drives,” 2008.
- [2] Bhim Singh and Sanjeev Singh, “State of the art on permanent magnet brushless DC motor drives,” *Journal of Power Electronics*, Vol. 9, No. 1, Jan 2009.
- [3] H. Li, S. Zheng, and H. Ren, “Self-correction of commutation point for high-speed sensorless BLDC motor with low inductance and nonideal back EMF,” *IEEE Trans. Power Electron.*, vol. 32, no. 1, pp. 642–651, Jan. 2017.
- [4] Park, J. S., Lee, K., Lee, S. G., & Kim, W. (2019). Unbalanced ZCP Compensation Method for Position Sensorless BLDC Motor. *IEEE Transactions on Power Electronics*, 34(4), 3020-3024. doi:10.1109/tpel.2018.2868828
- [5] T. M. Jahns, R. C. Becerra, and M. Ehsani, “Integrated current regulation for a brushless ECM drive,” *IEEE Trans. Power Electron.*, vol. 6, no. 1, pp. 118–126, Jan. 1991.
- [6] N. Ertugrul and P. Acarnley, “A new algorithm for sensorless operation of permanent magnet motors,” *IEEE Trans. Ind. Appl.*, vol. 30, no. 1, pp. 126–133, Jan./Feb. 1994.
- [7] R. Wu and G. R. Slemon, “A permanent magnet motor drive without a shaft sensor,” *IEEE Trans. Ind. Appl.*, vol. 27, no. 5, pp. 1005–1011, Sep./Oct. 1991.
- [8] S. Ogasawara and H. Akagi, “An approach to position sensorless drive for brushless dc motors,” *IEEE Trans. Ind. Appl.*, vol. 27, no. 5, pp. 928–933, Sep./Oct. 1991.
- [9] Y. Wang, X. Zhang, X. Yuan, and G. Liu, “Position-sensorless hybrid sliding-mode control of electric vehicles with brushless DC motor,” *IEEE Trans. Veh. Technol.*, vol. 60, no. 2, pp. 421–432, Feb. 2011.
- [10] C.-T. Lin, C.-W. Hung, and C.-W. Liu, “Sensorless control for four-switch three-phase brushless DC motor drive,” in *Proc. Conf. Rec. IEEE IAS Annu. Meeting*, 2006, vol. 4, pp. 2048–2053.
- [11] Kim, S. (2017). *Electric motor control: DC, AC and BLDC motors*. Cambridge, MA: Elsevier.
- [12] Rashid, M. H. (2014). *Power electronics handbook: Devices, circuits, and applications*. Upper Saddle River, NJ: Prentice Hall.
- [13] Zope, Pankaj & Bhangale, Pravin & Suralkar, SR. (2012). Design and Implementation of Carrier Based Sinusoidal PWM Inverter. *International Journal of Science and Research (IJSR)*. 1. 129-133.
- [14] Aboadla, E. H., Khan, S., Habaebi, M. H., Gunawan, T., Hamidah, B. A., & Yaacob, M. B. (2016). Effect of modulation index of pulse width modulation inverter on Total Harmonic Distortion for Sinusoidal. 2016 International Conference on Intelligent Systems Engineering (ICISE).
- [15] Zhang, B., & Qiu, D. (2019). *M-Mode SVPWM Technique for Power Converters*. Singapore: Springer Singapore.

- [16] Zhang, B., & Qiu, D. (2019). M-Mode SVPWM Technique for Power Converters. Singapore: Springer Singapore.
- [17] V. Ioniță, E. Cazacu and L. Petrescu, "Effect of voltage harmonics on iron losses in magnetic cores with hysteresis," 2018 18th International Conference on Harmonics and Quality of Power (ICHQP), Ljubljana, 2018, pp. 1-5.
- [18] Y. L. Karnavas, A. S. Topalidis and M. Drakaki, "Development of a low cost brushless DC motor sensorless controller using dsPIC30F4011," 2018 7th International Conference on Modern Circuits and Systems Technologies (MOCASST), Thessaloniki, 2018, pp. 1-4.
- [19] S. Tsooulidis and A. N. Safacas, "Deployment of an Adaptable Sensorless Commutation Technique on BLDC Motor Drives Exploiting Zero Sequence Voltage," in IEEE Transactions on Industrial Electronics, vol. 62, no. 2, pp. 877-886, Feb. 2015.
- [20] S. R. Bowes, "Regular-sampled harmonic elimination/minimisation PWM techniques," Fifth Annual Proceedings on Applied Power Electronics Conference and Exposition, Los Angeles, CA, USA, 1990, pp. 532-540.
- [21] STMicroelectronics, Application Note AN1276 BLDC Motor Start Routine for the ST72141 Microcontroller,[Online].Available:<https://forums.parallax.com/discussion/download/%2083730&d=1312466087>
- [22] P. Champa, P. Somsiri, P. Wipasuramonton and P. Nakmahachalasint, "Initial Rotor Position Estimation for Sensorless Brushless DC Drives," in IEEE Transactions on Industry Applications, vol. 45, no. 4, pp. 1318-1324, July-aug. 2009.
- [23] S. Ogasawara and H. Akagi, "An approach to position sensorless drive for brushless DC motors," in IEEE Transactions on Industry Applications, vol. 27, no. 5, pp. 928-933, Sept.-Oct. 1991.
- [24] P. B. Schmidt, M. L. Gasperi, G. Ray and A. H. Wijenayake, "Initial rotor angle detection of a nonsalient pole permanent magnet synchronous machine," IAS '97. Conference Record of the 1997 IEEE Industry Applications Conference Thirty-Second IAS Annual Meeting, New Orleans, LA, USA, 1997, pp. 459-463 vol.1.
- [25] G. H. Jang, J. H. Park, and J. H. Chang, "Position detection and startup algorithm of a rotor in a sensorless BLDC motor utilizing inductance variation," Proc. Inst. Elect. Eng.—Elect. Power Appl., vol. 149, no. 2, pp. 137–142, Mar. 2002
- [26] W.-J. Lee and S.-K. Sul, "A new starting method of BLDC motors without position sensor," *IEEE Trans. Ind. Appl.*, vol. 42, no. 6, pp. 1532–1538, Nov./Dec. 2006.
- [27] Y.-S. Lai, F.-S. Shyu, and S. S. Tseng, "New initial position detection for three-phase brushless DC motor without position and current sensors," *IEEE Trans. Ind. Appl.*, vol. 39, no. 2, pp. 485–491, Mar./Apr. 2003.
- [28] J. Sugawara, T. Kaimori, and S. Nichikata, "A novel and simple initial rotor position detecting method for PMSMs," in *Proc. IEEE PEDS*, 2005, pp. 612–617.

[29] Texas Instruments, “DRV10983 12- to 24-V, Three-Phase, Sensorless BLDC Motor Driver”, [Online]. Available: https://www.ti.com/lit/ds/symlink/drv10983.pdf?ts=1605653258006&ref_url=https%253A%252F%252Fwww.ti.com%252Fproduct%252FDRV10983%253FkeyMatch%253D DRV10983%2526tisearch%253DSearch-EN-everything%2526usecase%253DGPN